Parkinson's disease-derived α-Synuclein assemblies combined with chronic-type inflammatory cues promote a neurotoxic microglial phenotype

Cansu Yildirim[1,2,3,4], Alexis Fenyi[5], Pierre Besnault[1,2,3,4], Lina Gomez[1,2,3,4], Julia E. Sepulveda-Diaz[1,2,3,4], Patrick P. Michel[1,2,3,4], Ronald Melki[5], Stéphane Hunot[1,2,3,4]

[1]Sorbonne Université, Paris, France; [2]Institut du Cerveau - Paris Brain Institute - ICM, Paris, France; [3]Inserm UMRS 1127, Paris, France; [4]CNRS UMR 7225, Paris, France; [5]Institut François Jacob, MIRCen, CEA and Laboratory of Neurodegenerative Diseases, CNRS, 92265 Fontenay-aux-Roses, France

Corresponding author: Dr. Stephane Hunot
Paris Brain Institute – ICM, Hôpital de la Salpêtrière, 91 Bd de l'Hôpital, 75013 Paris, France
stephane.hunot@icm-institute.org

Keywords: Microglia; Parkinson's disease, α-Synuclein; Chronic inflammation; Neurotoxicity; Transcriptomic, Metabolomic, Cystine/glutamate transporter; Iron metabolism; Protein misfolding cyclic amplification

Abbreviations:

ACM	astrocyte-conditioned medium
aSYN	alpha-Synuclein
DIV	day *in vitro*
DLB	dementia with Lewy bodies
DN	dopaminergic neuron
DAM	disease-associated microglia
$DMEM^S$	supplemented Dulbecco's modified Eagle medium
F^S	*de novo*-generated aSYN fibrils
F^{PD}	PD patient-derived aSYN fibrils
F^{DLB}	DLB patient-derived aSYN fibrils
iMG	induced microglia-like cell
L-15	Leibovitz's L-15 medium
LP	Lewy pathology
LPS	lipopolysaccharide
M1	type-1 macrophage
M2	type-2 macrophage
MCM	microglia-conditioned medium
MSA	multiple system atrophy
Nb^S	supplemented neurobasal-A medium
ND	nondifferentiated
NSC	nonstimulated cells
PD	Parkinson's disease
PGE_2	prostaglandin E_2
PMCA	protein misfolding cyclic amplification
ROS	reactive oxygen species

TEM	transmission electron microscopy
TLR	toll-like receptor
TNFα	tumor necrosis factor alpha
TPF^{PD}	TNFα, PGE_2, F^{PD}
TPP	TNFα, PGE_2, Pam3CSK4

Abstract

Parkinson's disease (PD) is a common age-related neurodegenerative disorder characterized by the aggregation of α-synuclein (αSYN) building up intraneuronal inclusions termed Lewy pathology. Mounting evidence suggests that neuron-released αSYN aggregates could be central to microglial activation, which in turn mounts and orchestrates neuroinflammatory processes potentially harmful to neurons. Therefore, understanding the mechanisms that drive microglial cell activation, polarization and function in PD might have important therapeutic implications. Here, using primary microglia, we investigated the inflammatory potential of pure αSYN fibrils derived from PD patients. We further explored and characterized microglial cell responses to a chronic-type inflammatory stimulation combining PD patient-derived αSYN fibrils (F^{PD}), Tumor necrosis factor-α (TNFα) and prostaglandin E_2 (PGE_2) (TPF^{PD}). We showed that F^{PD} hold stronger inflammatory potency than pure αSYN fibrils generated *de novo*. When combined with TNFα and PGE_2, F^{PD} polarizes microglia toward a particular functional phenotype departing from F^{PD}-treated cells and featuring lower inflammatory cytokine and higher glutamate release. Whereas metabolomic studies showed that TPF^{PD}-exposed microglia were closely related to classically activated M1 proinflammatory cells, notably with similar tricarboxylic acid cycle disruption, transcriptomic analysis revealed that TPF^{PD}-activated microglia assume a unique molecular signature highlighting upregulation of genes involved in glutathione and iron metabolisms. In particular, TPF^{PD}-specific upregulation of *Slc7a11* (which encodes the cystine-glutamate antiporter xCT) was consistent with the increased glutamate response and cytotoxic activity of these cells toward midbrain dopaminergic neurons *in vitro*. Together, these data further extend the structure-pathological relationship of αSYN fibrillar polymorphs to their innate immune properties and demonstrate that PD-derived αSYN fibrils, TNFα and PGE_2 act in concert to drive

76 microglial cell activation toward a specific and highly neurotoxic chronic-type inflammatory
77 phenotype characterized by robust glutamate release and iron retention.
78

79 **Introduction**

80 Parkinson's disease (PD) is a common and multisystem neurodegenerative disorder characterized by
81 both motor and nonmotor symptoms. The neuropathological hallmark of PD is the progressive and
82 massive degeneration of dopaminergic neurons (DNs) in the *substantia nigra* associated with α-
83 Synuclein (αSYN)-rich deposits building up cytoplasmic inclusions known as Lewy pathology (LP). The
84 aggregation of αSYN may promote several molecular and biochemical defects affecting key cellular
85 functions and driving the progressive demise of DNs [1]. In addition to these toxic cell-autonomous
86 mechanisms, pathological αSYN assemblies can also spread from cell to cell to seed aggregate
87 formation in newly contaminated neurons. This prion-like mechanism is believed to contribute to the
88 progression of αSYN pathology across brain networks over time and to be linked to the progressive
89 clinical deterioration of patients [2, 3]. Accordingly, released extracellular αSYN aggregates may
90 directly interact with and activate surrounding glial cells including microglia to initiate a deleterious
91 inflammatory response. Indeed, evidence from epidemiological, *postmortem*, and animal studies
92 suggests that neuroinflammatory processes associated with glial and immune cell activation
93 participate in the progression of DN cell death [4].
94 Microglia, the most abundant tissue macrophages in the brain, execute numerous physiological
95 functions important for the maintenance of tissue homeostasis, synapse remodeling, neurotrophic
96 factor secretion and clearance of debris. However, under neurodegenerative conditions, and more
97 particularly upon chronic exposure to aberrant proteins, microglial cells mount persistent sterile (as
98 opposed to infectious) and proinflammatory immune responses [5]. In PD, major progress in our
99 understanding of microglial cell activation and related inflammation has shown that αSYN assemblies
100 behave as true molecular motifs associated with microbes (pathogen-associated molecular patterns
101 or PAMPs). These motifs are recognized by innate immune cells thanks to a panel of immune

102 receptors recognizing these molecular patterns (pattern recognition receptors or PRRs) such as Toll-
103 like receptors (TLRs). Thus, mounting evidence suggests that neuron-released αSYN assemblies could
104 be central to microglial cell activation and pathological inflammatory responses through the
105 activation of TLRs and other immune-related receptors including CD36 [6-9]. However, these studies
106 also revealed that the set of receptors involved in this activation crucially depends on the type of
107 αSYN assemblies used in the different experimental setups. Indeed, αSYN can assemble into
108 structurally distinct fibrillar assemblies (also termed polymorphs or strains) that exhibit different
109 phenotypic traits [10-12]. As we previously showed, these strains exhibit distinct spreading, tropism,
110 clearance, and neurotoxicity in cells and in the rodent brain, which might explain the pathological
111 and phenotypic diversity of different synucleinopathies such as PD, multiple system atrophy and
112 dementia with Lewy bodies [10-14]. Importantly, we recently strengthened this concept using
113 patient-derived αSYN strains generated by protein misfolding cyclic amplification (PMCA) [15].
114 Besides demonstrating a structure-pathology relationship we brought evidence for differences
115 between patient-derived and *de novo*-generated αSYN strains [15]. Taken together, these data
116 suggest that the intrinsic structure of fibrillar αSYN is a major determinant of its biological properties.
117 A likely explanation for this structure-function relationship is that differences in surface accessibility
118 contribute to the differential binding of distinct αSYN strains to partner proteins such as cell surface
119 receptors [12, 16]. Hence, whether patient-derived αSYN strains exhibit inflammatory activity similar
120 to or different from that of previously described *de novo*-generated αSYN polymorphs is unknown,
121 but their use in model systems has the potential to better model disease-associated microglial
122 activation and perhaps contribute to more relevant knowledge.

123 An often neglected, but important issue for understanding the pathomechanisms linked to innate
124 inflammation in PD is to comprehensively define the complex network of stimuli that drive microglial
125 cell activation and function. Most cell culture models for studying microglia-associated immunity in
126 PD have been developed upon exposure of microglia to the prototypical bacterial inflammogen
127 lipopolysaccharide (LPS) or, much elegantly, to different types of recombinant αSYN aggregates of

128 various purities as disease-specific triggers and TLR-activating pathological ligands [8, 9, 17, 18].
129 Although these models have brought invaluable knowledge about the molecular mechanisms and
130 pathways involved in microglial cell activation, they are limited in that they do not consider specific
131 aspects of PD-related neuroinflammation which is chronic in nature and most likely involves the
132 combined action of several mediators in the inflammatory milieu. It is now well established that the
133 phenotypes and functions that activated microglia can adopt are diverse and strongly depend on the
134 nature, intensity and complexity of stimulation in response to various cues [19]. Far from the original
135 idea that macrophages can be polarized into classically (M1) or alternatively (M2) activated cells
136 representing two polar extremes of molecular programming, there is now compelling evidence
137 suggesting that they can adopt a much larger spectrum of activation states associated with different
138 phenotypes and, presumably, functions [20, 21]. Notably, it has been shown that human
139 macrophages engage in a specific molecular program and adopt a unique phenotype when exposed
140 to a chronic-type inflammatory stimulus composed of Tumor necrosis factor (TNF)-α, prostaglandin
141 E_2 (PGE_2) and TLR2 ligands such as the synthetic molecule Pam3CSK4 (referred to as "TPP"
142 stimulation) [21]. These inflammatory factors are commonly found in chronic inflammatory
143 conditions such as *Mycobacterium tuberculosis*-associated granulomatous diseases or granulomatous
144 listeriosis [22-26]. Remarkably, the expression of these factors is elevated in the brains of PD patients
145 as well; αSYN aggregates being the most likely pathological ligand of TLR2 whose expression is tightly
146 linked to PD pathogenesis [27-29], suggesting that they may act in concert to shape microglial
147 activation into a unique disease phenotype. Yet, cell-specific immune properties might be important
148 and whether microglial cells behave similarly to peripheral macrophages upon chronic-type
149 inflammatory stimulation has not been explored.

150 In this study, using a model system of cultured primary microglial cells, we sought to document the
151 inflammatory properties of patient-derived αSYN strains and to determine whether microglia
152 exposed to PD-relevant inflammatory cues in a novel and original combinatory approach adopt a
153 specific molecular phenotype and function. We found that PD patient-derived αSYN fibrils hold

154 stronger inflammatory properties than αSYN fibrils assembled *de novo*. We also showed that,
155 compared to classical M1-shaped microglia (LPS-induced), cells simultaneously exposed to PD
156 patient-derived fibrils, TNFα and PGE_2 assume a unique chronic-type inflammatory molecular
157 signature associated with increased glutamate release and iron retention propensities as well as
158 higher neurotoxic activity.
159

160 **Methods**

161 **Animals**

162 Animal care and housing were conducted in accordance with the recommendations of the European
163 Union Council Directives (2010/63/EU). C57BL/6J mice were obtained from Janvier LABS (Le Genest
164 St Isle, France).

165 **Reagents and antibodies**

166 Leibovitz's L-15 medium (Thermo Fisher Scientific, Illkirch, France, #11415049), Dulbecco's Modified
167 Eagle Medium/F-12 nutrient mixture (DMEM; Thermo Fisher Scientific, #31885023), Neurobasal-A
168 medium (Nb; Thermo Fisher Scientific, #10888022), B27 supplement minus antioxidants (Thermo
169 Fisher Scientific, #10889038), N2 mix (Thermo Fisher Scientific, #17502048), RPMI-1640 Glutamax
170 (Invitrogen, #61870010), RPMI-1640 (Thermo Fisher Scientific, #21875034), penicillin/streptomycin
171 (Thermo Fisher Scientific, #15140122), antibiotic/antimycotic solution (Invitrogen, #15240062),
172 Trypsin 0.05% EDTA (Thermo Fisher Scientific, #25300054), polyethylenimine (PEI; Sigma Aldrich,
173 #P3143), Histopaque-1077 (Sigma Aldrich, #10771-500M), fetal bovine serum (FBS; Biowest, #S1820-
174 500), Nitrotetrazolium Blue chloride (Sigma Aldrich, #N6876), Pam3CSK4 (Invivogen, tlrl-pms),
175 Lipopolysaccharides (LPS) from *Escherichia coli* O26:B6 (Sigma-Aldrich, #L8274), recombinant human
176 TNFα (Sigma Aldrich, #H8916), PGE_2 (Sigma Aldrich, #P6532), recombinant mouse IFNγ
177 (Immunotools, #12343537), recombinant mouse IL4 (Immunotools, #12340045), recombinant human
178 GM-CSF (R&D, #215-GM-010), recombinant human IL34 (R&D, #5265-IL-010), Sulfasalazine (Sigma
179 Aldrich, S0883), MK-801 (Tocris, #0924), Cytotoxicity Detection Kit (LDH; Roche, #11644793001),

180 Amplex Red Glutamic Acid/Glutamate Oxidase Kit (Thermo Fisher Scientific, #A12221), NucleoSpin
181 RNA XS, RNA purification kit (Macherey-Nagel, #740902.50), SYBR Green reactifs (LightCycler® 480
182 SYBR Green I Master; Roche, #04707516001), StraightFrom® LRSC CD14 MicroBead Kit (Miltenyi,
183 #130-117-026), MACS BSA Stock Solution (Miltenyi, #130-091-376), autoMACS® Rinsing Solution
184 (Miltenyi, #130-091-222). The following antibodies were used: anti-mouse CD25 (Bio-Rad,
185 MCA1260), anti-mouse CD11b (Bio-Rad, MCA74G), anti-human CCR2 (R&D Systems; MAB150-100),
186 anti-human CX3CR1 (Bio-Rad, AHP566). Mouse TNFα ELISA Kit (Thermo Fisher Scientific, BMS607-3),
187 Mouse IL6 ELISA Kit (Thermo Fisher Scientific, BMS603-2TWO), Mouse IL1β ELISA Kit (Thermo Fisher
188 Scientific, BMS6002), Mouse IL10 ELISA Kit (R&D Systems, M1000B), U-Plex (Meso Scale Discovery,
189 K15069L-1), Mouse Pro-Inflammatory 7-Plex Tissue (Meso Scale Discovery, K15012B-1), Mouse IL1α
190 ELISA Kit (Biolegend, #433404), Mouse CXCL5 ELISA Kit (R&D Systems, MX000), and Hoechst 33342
191 (Tocris, #5117).

192 **Human brain tissue collection and preparation of αSYN assemblies**

193 Brain tissues from patients suffering from PD (n=4) or DLB (n=4) were obtained at autopsy from the
194 UK Brain Bank (Imperial College London, UK). The clinicopathological description of the patients is
195 detailed elsewhere [15]. After histological identification of LP-rich regions, the cingulate cortex was
196 isolated from the brains and processed into brain homogenates. Patient-derived αSYN assemblies
197 were obtained by protein misfolding cyclic amplification (PMCA) as described elsewhere [15]. Briefly,
198 frozen brain tissues were diluted 1:5 (w/v) in PMCA buffer (150 mM KCl, 50 mM Tris–HCl pH 7.5) and
199 sonicated for 1 min, with 10 s pulses followed by 10 s pauses (SFX 150 Cell Disruptor sonicator
200 equipped with a 3.17 mm Branson microtip probe). Brain homogenates were further diluted in PMCA
201 buffer containing monomeric αSYN (100 µM) to a final concentration of 2% (w:v). PMCA
202 amplification (4 cycles) was performed using a Q700 generator and a 431MPX horn (Qsonica,
203 Newtown, CT, USA) with the following sequence: 15 s of sonication and 5 min pause at 31°C. Cycles
204 2, 3 and 4 were performed using 1% of the preceding cycle reaction as seeds. At cycle 4, the PMCA
205 reaction products were spun for 30 min at 50,000xg and the pelleted assemblies were resuspended

206 in phosphate-buffered saline (PBS) at a final concentration of 100 µM. Prior to usage, the assemblies
207 were fragmented by sonication for 20 min in 2-ml Eppendorf tubes in a Vial Tweeter powered by an
208 ultrasonic processor UIS250v (250 W, 2.4 kHz; Hielscher Ultrasonic, Teltow, Germany), aliquoted,
209 flash frozen in liquid nitrogen and stored at -80°C. Recombinant αSYN fibrils were prepared and
210 characterized as previously described (Bousset et al., 2013). We used the LALChromogenic Endotoxin
211 Quantitation Kit (Thermo Fisher catalog no. 88282) following manufacturer instructions and a
212 CLARIOstar Plus (BMG Labtech, Ortenberg, Germany) plate reader as described previously [13]. To
213 ascertain that the endotoxin levels were less than 0.015 endotoxin units/mg (EU/mg). In preliminary
214 studies, we observed similar inflammatory activities in cultured microglia from patient-derived αSYN
215 fibrils among patients in each disease group. Therefore, we prepared a single batch of PD and DLB
216 patient-derived αSYN fibrils by mixing equal amount of assemblies generated from the 4 patients in
217 each disease group.

218 **Transmission electron microscopy**

219 The morphology of the PMCA-amplified αSYN assemblies (3rd cycle) was assessed by transmission
220 electron microscopy (TEM) using a Jeol 1400 transmission electron microscope following adsorption
221 onto carbon-coated 200 mesh grids and negative staining with 1% uranyl acetate. The images were
222 acquired using a Gatan Orius CCD camera (Gatan, Elancourt, France).

223 **Primary mouse microglial culture**

224 Primary mouse microglia were isolated and cultured following a protocol previously described [30].
225 Newborn pups were sacrificed, and the whole brain was rapidly dissected. After mechanical
226 dissociation of the brain tissue, the cells in suspension were plated onto polyethyleneimine-coated T-
227 75 flasks with 12 ml of DMEM supplemented with 10% FBS and antibiotics (2 brains per flask). At
228 DIV2, the medium was completely changed to fresh medium, and the culture was subsequently left
229 to grow without changing the medium until microglial cell isolation was complete (DIV14–18). For
230 microglial-conditioned medium (MCM) transfer into neuronal culture media, microglia were grown
231 and stimulated in DMEM-based astrocyte-conditioned medium (ACM) prepared as described below.

232 **Microglial cell seeding and stimulation**

233 Cultured microglia were washed 3 times with DMEM and incubated for 5 min with 5 mL of
234 prewarmed (+37°C) trypsin. DMEM containing 10% FBS (10 mL) was then added to abrogate trypsin
235 activity, and the cells were collected in an ice-cold 50 mL falcon tube before centrifugation at 188 x g
236 for 6 min at 4°C. The cell pellet was then resuspended in DMEM-1% FBS. The cells were plated at a
237 density of 90,000 to 110,000 cells/cm^2 and incubated for 24 h at 37°C for complete settlement.
238 Microglia were stimulated for 24 to 48 hours with LPS (10 ng/mL), Pam3CSK4 (1 µg/mL), TNFα (800
239 IU/mL), PGE_2 (1 µg/mL) or fibrillar αSYN assemblies at various concentrations. When indicated,
240 stimulation factors were used in combination.

241 **Astrocyte-conditioned medium**

242 Astrocyte-conditioned medium (ACM) was prepared from primary cultures of astrocytes obtained
243 from C57BL/6J mouse neonate (P0) brains as described elsewhere [31]. Briefly, brains were dissected
244 and dissociated by mechanical trituration in L15 medium. After centrifugation, the cell pellet was
245 resuspended in DMEM/F-12 plus 10% FBS, and the dissociated cells were distributed and allowed to
246 grow on laminin-coated T-75 flasks. At DIV2, the medium was replaced with fresh DMEM/F-12 plus
247 10% FBS, and clodronate-loaded liposomes (2.6 µg/mL; Liposoma BV, Netherlands) were added twice
248 weekly to remove residual macrophages. Twelve to fourteen days later (DIV14-16), the culture
249 medium was completely removed and replaced with either DMEM or Nb supplemented with 2% B27,
250 1% N2 and 1% antibiotics (referred to as DMEM^S and Nb^S, respectively). After three additional days of
251 culture, the DMEM^S- and Nb^S-based ACM were recovered, sterilized with 0.2µm syringe filters and
252 frozen −20°C until use.

253 **Primary mouse midbrain culture**

254 Primary mouse midbrain cultures were prepared as described previously [31]. Briefly, embryos
255 (E13.5) from pregnant C57Bl6 females (Janvier LABS, Le Genest St Isle, France) were collected in L15
256 medium, and the midbrain was dissected under a binocular microscope. Midbrain tissue was
257 digested in Trypsin plus 0.05% EDTA (Thermo Fisher Scientific, #25300054) for 20 min at +37°C and

258 after neutralization of Trypsin with L15 supplemented with 10% fetal calf serum, predigested tissue
259 was then mechanically triturated by gentle pipetting (8–10 strokes) using a Gilson pipette fitted with
260 a sterile polypropylene blue tip with no filter (StarLab France, Orsay, France). After 10 min of
261 sedimentation on ice, the supernatant was collected, and the trituration and sedimentation steps
262 were repeated one more time. The collected supernatant was then centrifuged at 317xg for 5 min at
263 +4°C. The cell pellet was resuspended in L15 medium and dissociated cells were distributed in PEI-
264 coated Nunc 48-well plates (Roskilde, Denmark) in Nb^S at a density of 0.4 midbrains/well. After 1-2
265 hours incubation, ARA-C (1.2 µM; Sigma Aldrich, C1768) was added to curtail astrocyte proliferation.
266 At DIV 1, ARA-C was brought to a 1.6 µM final concentration and at DIV 2, the culture medium was
267 fully replaced by Nb^S-based ACM. The use of a conditioning step by astrocytes was shown to improve
268 the ability of Nb^S to promote the development and long-term viability of cultivated neurons [31, 32].

269 **Quantification of ROS levels**

270 To determine the intracellular production of superoxide anions upon stimulation we used nitro-blue
271 tetrazolium chloride (NBT) reagent following a protocol adapted from [33]. In brief, 100 000 cells
272 were seeded in 48-well plates and stimulated as described above for 24 hours. One and a half hours
273 before the assay, NBT (500 µM) was added to each well and the cells were further incubated before
274 they were washed twice with warm PBS at 24 hours after stimulation. Then, 100 µL of absolute
275 methanol was added to each well and the culture plates were left under the fume hood until
276 methanol evaporation. After complete drying, 60 µL of 2 M KOH and 70 µL of DMSO were added to
277 the wells and incubated under mild agitation for 5-10 minutes after the absorbance at 620 nm was
278 measured. The results were normalized to those of the NSC experimental condition.

279 **Cytokine and glutamate assays**

280 Cytokine levels were measured using ELISA kits or MSD U-Plex plates (Meso Scale Diagnostics)
281 according to the manufacturer's instructions. Glutamate levels were measured using an Amplex Red
282 Glutamic Acid/Glutamate Oxidase Kit according to the manufacturer's instructions. Quantification
283 was carried out on 10 µl of culture medium samples. The fluorescent reaction products resulting

284 from glutamic acid oxidation were quantified using excitation and emission wavelengths of 545 and
285 590 nm, respectively. Absorbance and fluorescence were measured using a SpectraMax i3X
286 microplate reader (Molecular Devices, Sunnyvale, CA).

287 **Transcriptomic analysis**

288 To determine the transcriptomic changes evoked by the different inflammatory stimuli, $1x10^5$
289 microglial cells were seeded in 48-well plates and then stimulated or not (NSC) with LPS (10 ng/ml) or
290 TPF^{PD} for 24 hours. Seven to eight biological replicates per condition from two independent
291 experiments were used. RNA was isolated using a NucleoSpin RNA XS Kit, and RNA quality was
292 evaluated with an Agilent 2100 Bioanalyzer (Agilent Technologies). All RNA samples had RNA
293 integrity numbers (RINs) greater than 7. We produced libraries for 3′-mRNA sequencing using 200 ng
294 of purified RNA per sample processed with a TruSeq Stranded RNA Kit (Illumina, San Diego, CA)
295 according to the manufacturer's protocol. Paired-end sequencing was subsequently performed on
296 the Illumina NextSeq 500 and NovaSeq 6000 platforms with a sequencing depth of 80 million reads
297 per sample (iGenSeq core facility, ICM, Paris France). All samples were assessed separately for overall
298 read quality using FASTQC. Reads were trimmed using the Trimmomatic tool (Illumina), and then
299 aligned to the mouse genome using Top-Hat (Illumina) and fragments were assigned to genes using
300 the FeatureCounts program (iCONICS core facility, ICM, Paris France). Differentially expressed genes
301 (DEGs) were analyzed using the open-source Bioconductor package DESeq2 in R software [34]
302 (log2FC > 0.5; FDR-adjusted p value < 0.05). Pathway enrichment analysis was performed using the
303 open-source gene enrichment analysis tool Enrichr [35-37]. Data visualization and biological
304 interpretation were performed with GraphPad Prism 7.0 software.

305 **Metabolomic analysis**

306 Metabolite profiling analysis was carried out on an Acquity UPLC system (Waters Corp, Saint-
307 Quentin-en-Yvelines, France) coupled to a hybrid Orbitrap- and Q Exactive-based instrument
308 (Thermo Fisher Scientific, Illkirch, France). To analyze and compare the microglial cell metabolome
309 under different inflammatory conditions, we performed an untargeted metabolomic analysis of cells

310 stimulated with or without LPS (10 ng/mL) or TPF^{PD} for 48 hours. Five biological replicates for each
311 condition were prepared. Approximately $1x10^6$ cells grown in $25cm^3$ flasks were lysed using a
312 methanol-based method consisting of adding 1 mL of frozen methanol (-20°C) followed by 5 min of
313 incubation on dry ice and 5 min of rest at room temperature. This incubation cycle was repeated 3
314 times before the cells were collected with the help of a cell scraper, after which the cells were
315 transferred to a 50 mL Falcon tube. The samples were kept frozen at -80°C until use. Sample
316 preparation for LC-MS analysis was as follows: Prior to extraction, cells were homogenized in 100 µL
317 of H_20 containing 0.1% formic acid and internal standards (a mixture of 16 labeled amino acids at 10
318 µg/mL) to a final concentration of 2500 cells/µl. Six cycles of freeze-thaw cycling were applied for cell
319 lysis. Then, 4 volumes of frozen methanol (−20°C) containing an equimolar (10 µg/mL) mixture of
320 internal standard [16 labeled amino acids and 3 labeled nucleotides (ATP,$^{15}N_5$; ADP,$^{15}N_5$ and
321 AMP,^{13}C,$^{15}N_5$)] were added to 100 µL of sample and vortexed. The samples were further sonicated
322 for 10 min before being centrifuged at 10,000×g and +4°C for 2 min and left for one hour (+4°C) for
323 slow protein precipitation. The samples were then centrifuged at 20,000×g (+4°C) for 20 min, after
324 which the supernatants were transferred to new tubes and subsequently dried before being
325 reconstituted in a solution of water/acetonitrile (40:60; v-v). The chromatographic conditions and
326 experimental settings were previously described [38]. Briefly, LC-MS analysis was performed with a
327 ZIC-*p*HILIC chromatographic column (5 µm, 2.1 × 150 mm, Merck, Darmstadt, Germany). Full scan
328 positive and negative ionization modes with a resolution of 70.000 (FWHM) and a scan range of m/z
329 50–750 were used. The mass spectrometer was systematically calibrated in both ion polarity modes
330 with Pierce calibration solution. The injection volume was set to 10 µL. The mobile phase (flow rate
331 of 0.2 mL/min for 29 min) consisted of 10 mM ammonium carbonate at pH=10.5 (A) and acetonitrile
332 (B). MS data processing was performed using the XCMS R package with the CentWave algorithm and
333 CAMERA tools implemented in R software and the galaxy workflow4metabolomics [39-41]. The
334 processing steps included peak picking, peak grouping, retention time correction and annotation of
335 isotopes and adducts. Processed LC-MS data were further analyzed based on standard protocols [42,

336 43], which resulted in a data matrix in which each metabolomic feature was characterized by a
337 retention time (RT), a mass-to-charge ratio (m/z), its corresponding intensities and the isotope-
338 adduct annotation from the CAMERA tool. The metabolomics data matrix was then filtered,
339 normalized, curated and log-10 transformed based on a quality assurance (QA) strategy [44, 45].
340 Notably, peaks with more than 30% of missing values were discarded. Data visualization for biological
341 interpretation was performed with the Multi Experiment Viewer (MeV) statistical software package
342 (version 4.9.0; http://www.tm4.org/mev/) [44]. This software was used to perform principal
343 component analysis (PCA), heatmaps and tests to compute a p-value for each metabolic feature with
344 a threshold of significance set to 0.05. False discovery rates (FDRs) were corrected using the
345 Benjamini-Hochberg method [47] to adjust p-values for false discovery involving multiple
346 comparisons.

347 **Quantitative real-time PCR**

348 Total RNA was isolated using an extraction kit according to the manufacturer's instructions
349 (Macherey-Nagel). The RNA concentration was assayed with a NanoDrop (Thermo Scientific) and
350 adjusted with nuclease-free water to an equal concentration for all samples. RNA was then reverse
351 transcribed to cDNA using the Verso cDNA Synthesis Kit (Thermo Scientific) following the
352 manufacturer's instructions. In brief, RNA was denatured at 70°C for 2 min. Then, the kit mixture was
353 added to each tube. The samples were subjected to successive incubations at 25°C for 10 min, 42°C
354 for 1 h and 85°C for 5 min.

355 A quantitative PCR assay was designed to include three technical replicates per sample and two
356 reference genes (*Rab7* and *Sdha* for primary mouse microglia; *Ubc* and *Sdha* for human microglia-like
357 cells) which were selected upon analysis of gene expression stability across the different
358 experimental conditions (geNorm tool of qBasePlus software, Biogazelle) and among the 8-10 initial
359 gene candidates. Quantitative PCR was performed using a LightCycler® 480 System with compatible
360 SYBR Green reagents (LightCycler® 480 SYBR Green I Master). The PCR program was 95°C for 10 min,

361 45 cycles of 95°C for 15 sec and 60°C for 60 sec and cooling. All the generated data were further
362 processed and analyzed with qBasePlus.

363 **Generation of human induced microglia-like cells**

364 Blood samples were collected from a healthy donor (49-year-old male) who provided signed
365 informed consent and who was included in an INSERM-sponsored clinical study. Human induced
366 microglia-like cells (iMGs) were obtained following the protocol published by [48] with some
367 modifications. Briefly, 10 mL blood samples were collected in EDTA, and peripheral blood
368 mononuclear cells (PBMCs) were purified by density gradient (Histopaque-1077) centrifugation at
369 400xg for 30 min. After isolation, the cells were washed in RPMI-1640 medium and centrifuged at
370 300xg for 10 min. The cell pellet was resuspended in separation buffer (MACS BSA stock
371 solution/AutoMACS® Rinsing Solution at 1/20 dilution) and passed through MACS SmartStrainers (30
372 µm) to eliminate cell clumps. Monocytes were then isolated using 250 µL of MicroBeads-conjugated
373 human CD14 antibodies (StraightFrom LRSC CD14 MicroBead Kit; Miltenyi Biotec) added to 40 mL of
374 cell suspension. The cells and beads were incubated for 15 min at +4°C and centrifuged at 300xg for
375 10 min. The cell pellet was resuspended in the separation buffer and the labelled cells were
376 separated by LS columns on a QuadroMACS™ Separator and recovered in whole-blood column
377 elution buffer. After centrifugation at 300xg for 10 min, the cell pellet was resuspended in RPMI-1640
378 GlutaMAX supplemented with 10% FBS and 1% antibiotic-antimycotic solution. Monocytes were then
379 seeded at a concentration of $6x10^4$ cells/well in 96-well plates and incubated overnight at 37°C with
380 5% CO_2. To induce differentiation, the medium was changed at DIV1 with RPMI-1640 GlutaMAX
381 containing recombinant human GM-CSF (10 ng/ml) and recombinant human IL34 (100 ng/ml). The
382 differentiating medium was freshly renewed at DIV6. On day 27 following cell seeding, differentiated
383 iMGs were subjected to an inflammatory stimulation assay.

384 **Cell immunostaining and quantification**

385 Primary microglia and iMGs were fixed with 3.7% formaldehyde solution (Sigma Aldrich, 252549) for
386 12 min and then washed twice with PBS. Primary mouse microglia were then incubated overnight at

387 +4°C with rat anti-CD25 (1/100) or rat anti-CD11b (1/100) antibodies diluted in PBS. Then, cells were
388 washed three times with PBS and incubated with anti-rat IgG coupled with Alexa488 fluorophore
389 (1/300 dilution) for 2 hours at RT. For double immunofluorescence staining of iMGs, cells were
390 incubated overnight at +4°C with rabbit anti-CX3CR1 and mouse anti-CCR2 primary antibodies
391 (diluted 1/500 in PBS containing 0.1% Triton-X 100 and 5% NGS). The cells were then rinsed three
392 times with PBS and incubated with anti-rabbit IgG conjugated to the Alexa488 fluorophore and anti-
393 mouse IgG conjugated to the Alexa546 fluorophore (1/300 dilution) for 1 hour at RT. After two
394 washes with PBS, the immunostained cells were further stained with Hoechst (1/4000 dilution) for 10
395 min and rinsed three additional times with PBS. The ratio of CX3CR1 to CCR2 was calculated by
396 quantifying the fluorescent signal intensity using an automated quantitative imaging platform
397 (ArrayScan, Thermo Fisher). Representative images were acquired using an Axio Observer
398 7/Apotome microscope (Zeiss). For midbrain cultures, a similar immunodetection protocol was used
399 to assess tyrosine hydroxylase (TH), a dopaminergic neuronal marker. The cells were incubated at
400 +4°C for 24 hours in mouse anti-TH primary antibodies (LNC1; Immunostar, #22941) diluted 1/2500
401 in PBS plus 0.2% Triton-X 100. The cells were then rinsed three times and incubated for 2 hours at
402 room temperature in Alexa Fluor 488-conjugated goat anti-mouse secondary antibodies (1/300
403 dilution; Thermo Fischer Scientific). Following two washes in PBS, cells were stained with Hoechst
404 33342 (1/4000 dilution; Tocris, 5117) for 10 min. Neuron culture images were acquired with a Nikon
405 Eclipse Ti-U fluorescence inverted microscope (Nikon France, Champigny sur Marne, France)
406 equipped with a Hamamatsu's ORCA-D2 camera and HCImage software (Hamamatsu Photonics,
407 Massy, France). The number of TH+ neurons/culture well was estimated by visually inspecting
408 samples with a 10× objective over 10–15 visual fields that were randomly selected for each
409 treatment condition.

410 **Statistical analysis**

411 Statistics were analyzed using SigmaPlot 14.0 or GraphPad Prism 7.0 software. The results are
412 expressed as the means ± standard errors of the means (SEM). The normality of data distribution was

413 assessed with the Shapiro-Wilk test. Statistical significance of normally distributed data was assessed
414 using Student's t-test for comparisons between two groups and ANOVA followed by Tukey's post-hoc
415 test for multiple comparisons. When the data were not normally distributed, significance was
416 determined with Mann-Whitney U test for comparisons of two groups and Kruskal-Walli's test
417 followed by Dunn's test for multiple comparisons. The statistical significance level was set as follows:
418 * *p* value < 0.05, ** *p* value < 0.01, and *** p value < 0.001.
419

420 **Results**

421 **Generation and characterization of patient-derived αSYN assemblies**

422 To investigate the inflammatory properties of patient-derived αSYN aggregates we first generated
423 pure *in vitro* amplified αSYN fibrillar assemblies using a protein misfolding cyclic amplification assay
424 (PMCA) applied to LP-rich PD and DLB brain tissue homogenates as described elsewhere [15]. A
425 detailed structural and biochemical characterization of this PMCA-amplified pathological material
426 demonstrated that fibrillary assemblies derived from PD patients (F^{PD}) are structurally different from
427 those obtained from DLB patients (F^{DLB}). Thus, TEM analysis revealed disease-specific differences in
428 the shape of the fibrils with PD patient-derived αSYN fibrils exhibiting a relatively flat and twisted
429 appearance whereas those derived from DLB patients were cylindrical exhibiting no twists
430 (Additional File 1: Fig. S1). Furthermore, assemblies from individual PD or DLB patients had distinct
431 limited proteolysis patterns suggesting the existence of disease-specific αSYN strains [15].
432

433 **PD-derived αSYN assemblies evoke robust inflammatory response in primary microglial cells**

434 We evaluated and compared the inflammatory potential of PD patient-derived αSYN fibrils by
435 exposing primary microglial cells to equal concentrations (3µM) of either F^{PD} or well-characterized
436 αSYN fibrils generated *de novo* (F^{S}) [8, 10]. As a positive control for inflammatory microglia, cells
437 were treated with LPS (10 ng/ml), a prototypical inflammogen and ligand for TLR4 [49]. After 48
438 hours of treatment, stimulated microglia undergo morphological changes as compared to non-

439 stimulated control cells (NSC) (Fig. 1A). In particular, LPS-exposed cells lose their ramified and
440 spindle-shaped processes adopting more flattened and wider morphologies typical of inflammatory
441 induction [30]. Of note, F^{S} and F^{PD} treatment induced morphological changes similar to those
442 observed with LPS stimulation suggesting inflammatory activation by αSYN fibrillar assemblies. To
443 obtain further insights into the inflammatory potential of F^{PD}, we evaluated the production and
444 release of several inflammatory cytokines in response to increasing amounts of F^{PD} ranging from 0.01
445 to 3 µM. We observed a dose-dependent increase in the release of TNFα, IL6 and IL10 after 24 hours
446 of treatment (Fig. 1B), with efficient and significant cytokine release occurring at F^{PD} concentrations
447 of 1 µM and above (Fig. 1B). As inflammatory microglia, particularly when exposed to fibrillary
448 aggregates of αSYN, can release large amounts of glutamate [50], we measured glutamate
449 concentrations in microglial cell culture medium after exposure to F^{PD}. As shown in Figure 1B, F^{PD}
450 strongly promoted glutamate release from microglia in a dose-dependent manner within the F^{PD}
451 concentration range of 1.5 and 3 µM (3- and 11-fold increases, respectively, compared to those of
452 NSCs). Whereas both F^{PD} and F^{S} efficiently triggered inflammatory-associated morphological changes
453 in microglial cells (Fig. 1A), we found that F^{PD} was more potent than F^{S} at inducing cytokine and
454 glutamate release after 48 hours of stimulation. Indeed, at an equal concentration of αSYN
455 assemblies (3µM), F^{PD} induced 5-, 17- and 3-fold more TNFα, IL6 and IL10 than F^{S}, respectively (Fig.
456 1C). Similarly, the extracellular amount of glutamate following exposure to F^{PD} was twice as high as
457 that in F^{S}-stimulated cells (Fig. 1C). Interestingly, we observed that microglia-associated inflammatory
458 responsiveness toward F^{DLB} was even more important than that evoked by F^{PD} assemblies (Fig. 1C).
459 Together, our data not only show that F^{PD} has potent inflammatory effects on microglial cells but also
460 that PD-derived assemblies exhibit stronger and weaker stimulatory effects than αSYN fibrils
461 generated *de novo* and from F^{DLB}, respectively. Given the structural differences between F^{PD} and F^{S},
462 and between F^{PD} and F^{DLB} [10, 15], our data also suggest a structure-function relationship regarding
463 the inflammatory properties of αSYN aggregates on brain tissue macrophages and argue for the use
464 of PD-derived material to better model disease-associated inflammatory mechanisms.

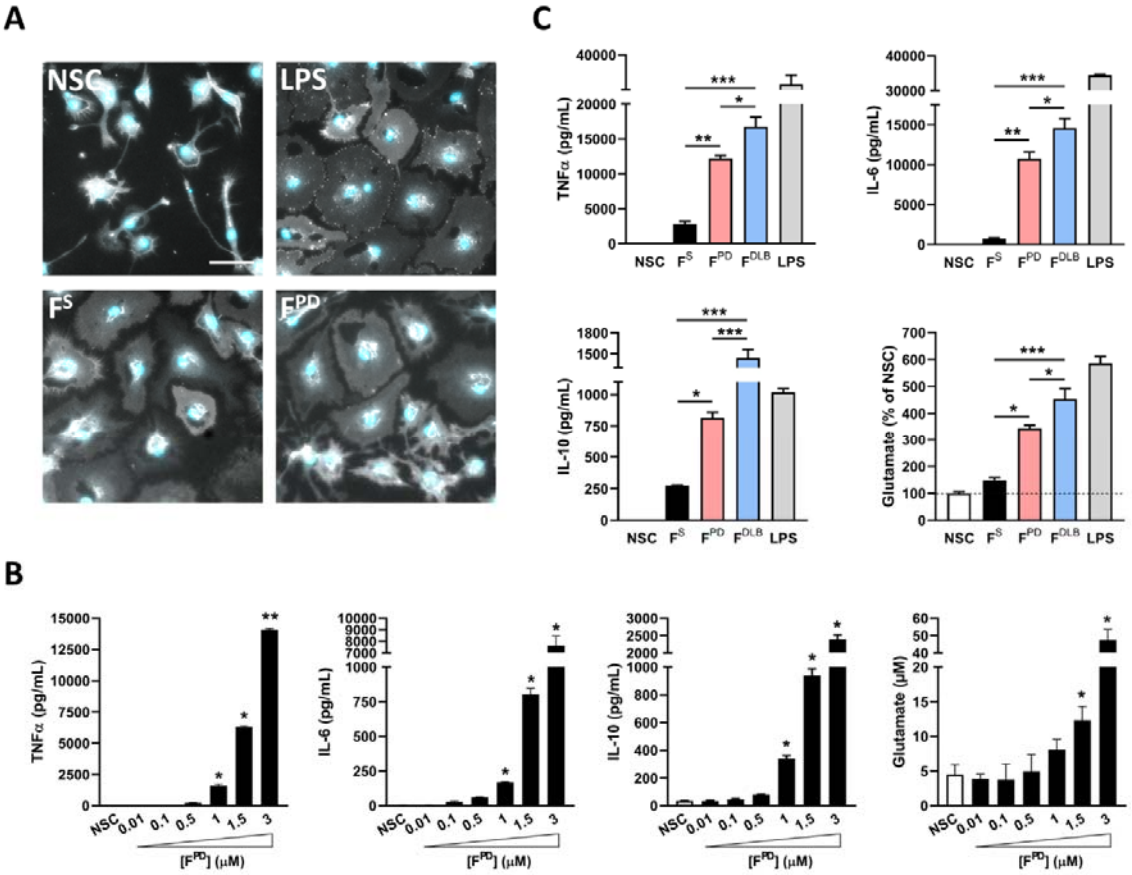

Figure 1. aSYN fibrils derived from PD patients hold more potent inflammatory properties than *de novo*-generated counterparts. (**A**) Representative images of CD11b immunostaining and Hoechst nuclear staining (blue) showing the morphological changes in microglial cells following inflammatory stimulation by the prototypal inflammogen LPS (10 ng/ml), *de novo* assembled human αSYN fibrils (3 µM; F^S) and fibrils derived from PD patients (3 µM; F^{PD}). Note that inflammatory stimulation results in cellular flattening and shortening of cell processes under all three inflammatory conditions. Scale bar: 50 µm. (**B**) Dose-response analysis of TNFα, IL6, IL10 and glutamate release by microglial cells exposed or not (NSC) to increasing concentrations (from 0.01 to 3 µM) of αSYN fibrils derived from PD patients (F^{PD}). The data are presented as the means ± SEM (n = 6). *p < 0.05; **p < 0.01 vs. NSC (Tukey's test). (**C**) Quantification of TNFα, IL6, IL10 and glutamate release by microglial cells exposed or not (NSC) to similar concentrations of F^S, F^{PD} or F^{DLB} (3 µM). The data are presented as the means ± SEM (n = 6). *p < 0.05; **p < 0.01; ***p < 0.001 vs. F^S (Tukey's test).

478 **Chronic-type stimulation of microglia is associated with decreased cytokine levels but increased**
479 **glutamate release.**
480 Chronic inflammatory conditions in humans are associated with sustained high tissue levels of TNFα,
481 PGE_2 and innate immune receptor-activating ligands that act in concert to shape the macrophage
482 response. Combinatory stimulation of human macrophages with these factors (the so-called TPP
483 stimulation) results in a specific molecular pattern and phenotype that departs from the well-
484 established classical M1 and alternative M2 activation state axis [21]. In particular, the cell-surface
485 markers CD25, CD14 and CD23 as well as the cytokine IL1α and, to a lesser extent, the chemokine
486 CXCL5 were found to be induced in TPP-specific conditions [21]. Remarkably, elevated levels of both
487 TNFα and PGE_2 have been documented in the *substantia nigra* of PD patients, suggesting that these
488 inflammatory mediators might act in concert with TLR-activating pathological αSYN aggregates to
489 drive microglial cell polarization toward a specific disease phenotype. Therefore, in an effort to
490 better model chronic-type PD innate immune response, we sought to integrate these disease-
491 relevant inflammatory cues together with αSYN fibrils, the presumed primary pathological trigger.
492 We first tested whether microglial cells would respond similarly to peripheral macrophages upon
493 chronic-type inflammatory stimulation as previously described [21]. Indeed, while peripheral
494 macrophages and microglia share an origin in the yolk sac, microglia are an ontogenetically distinct
495 cell population, so their responsiveness to chronic-type inflammatory stimulation may not exactly
496 mirror that of their macrophage relatives [51]. We thus investigated the expression of TPP-induced
497 immune markers in microglial cells exposed to a combination of TNFα (800 UI/ml), PGE_2 (1 μg/ml)
498 and the TLR2 agonist Pam3CSK4 (Pam3C; 1 μg/ml) compared to cells stimulated with conditions
499 linked to M1 (IFNγ; 20 ng/mL) or M2 (IL4; 10 ng/mL) polarization. Immunostaining for CD25 revealed
500 that, unlike peripheral macrophages, microglial cells not only express high basal levels of this cell-
501 surface marker but also exhibit unchanged expression under M2 and TPP stimulation, and
502 downregulation under M1 polarization (Fig. 2A). Similarly, whereas IL1α was specifically induced in
503 TPP-stimulated macrophages [21], it was only increased in M2-polarized (IL4-treated) microglial cells

504 (Fig. 2B). Finally, TPP-exposed microglia produced and released as much CXCL5 as did IL4-treated
505 cells, in contrast to the upregulation of this chemokine in both IFNγ- and TPP-stimulated human
506 macrophages (Fig. 2B). Notably, the poor or degraded biological activity of recombinant IFNγ was
507 unlikely to account for the apparent unresponsiveness of microglial cells to IFNγ-induced CXCL5 since
508 this treatment efficiently stimulated the intracellular production of reactive oxygen species (ROS) as
509 a consequence of NADPH-oxidase activation (Fig. 2C). Taken together, these data show that
510 microglial cells feature distinct TPP-associated gene regulation patterns compared to those of
511 peripheral macrophages.
512

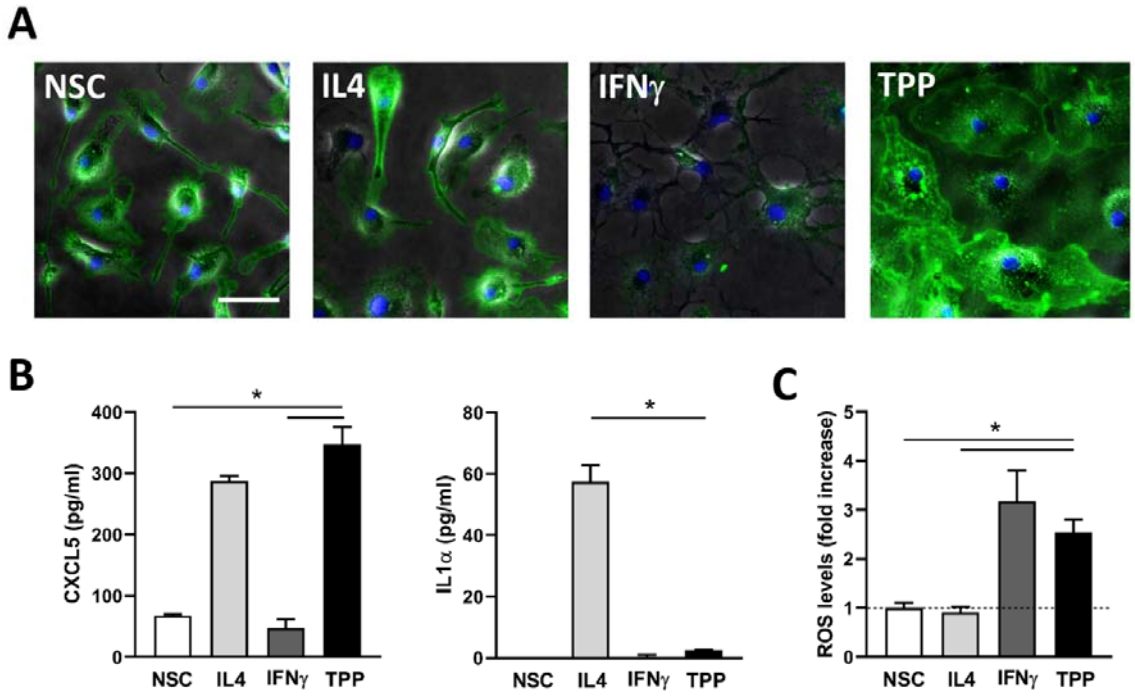

513

514 **Figure 2. Regulation of human macrophage-associated TPP-specific inflammatory markers in**
515 **microglial cells.** (**A**) Representative images showing CD25 immunostaining with Hoechst nuclear stain
516 (blue) in nonstimulated microglial cells (NSC) and cells exposed to IL4 (10 ng/mL), IFNγ (20 ng/mL) or
517 a combination of TNFα (800 UI/ml), PGE_2 (1 µg/ml) and Pam3C (1 µg/ml) (TPP stimulation). Scale bar:
518 60µm. (**B**) Quantification of CXCL5 and IL1α release by microglial cells exposed or not (NSC) to the
519 indicated treatments. Data are means ± SEM (n = 4). *p < 0.05 vs. TPP (Tukey's test). (**C**)

520 Quantification of ROS production measured via the NBT reaction in microglial cells exposed or not
521 (NSC) to the indicated treatments. The data are represented as the means ± SEM (n = 4).
522 *p < 0.05 vs. TPP (Tukey's test).

523

524 We next investigated the microglial cell response to chronic-type inflammatory stimulation by
525 implementing PD patients-derived αSYN fibrils (F^{PD}) to the treatment cocktail assuming that F^{PD}
526 would efficiently bind and activate microglial TLRs as demonstrated for αSYN fibrils made *de novo* [8,
527 52-55]. Using ELISA assay, we found that unlike LPS and F^{PD}, TNFα and PGE_2, alone or in combination
528 (TP), were ineffective at stimulating the release of TNFα, IL6, IL1β and IL10 after 48 hours of
529 treatment (Fig. 3A and B). Remarkably, cotreatment of F^{PD}-exposed cells with TNFα and PGE_2 (TPF^{PD}
530 stimulation) significantly suppressed cytokine released compared to that in cells treated with F^{PD}
531 alone, suggesting that chronic-type inflammatory stimulation is associated with a significantly but
532 less intensive inflammatory state. To determine whether TPF^{PD} stimulation is associated with an
533 overall reduction in the inflammatory grade of microglial cells, we measured and compared
534 intracellular ROS levels following the different treatments. Figure 3C shows that, unlike its effects on
535 cytokine production/release, TP did not mitigate F^{PD}-induced ROS generation in microglial cells. To
536 further investigate the inflammatory properties associated with TPF^{PD} stimulation, we analyzed
537 microglial glutamate release under these conditions. We observed that, unlike cytokine (decrease)
538 and ROS (unchanged) production, TPF^{PD} treatment was associated with a significant increase in
539 extracellular glutamate levels compared to F^{PD} treatment alone (Fig. 3D). Overall, our data show that,
540 upon chronic-type inflammatory stimulation, microglial cells adopt a nonconventional phenotype
541 rather than the classical proinflammatory M1 state.

542

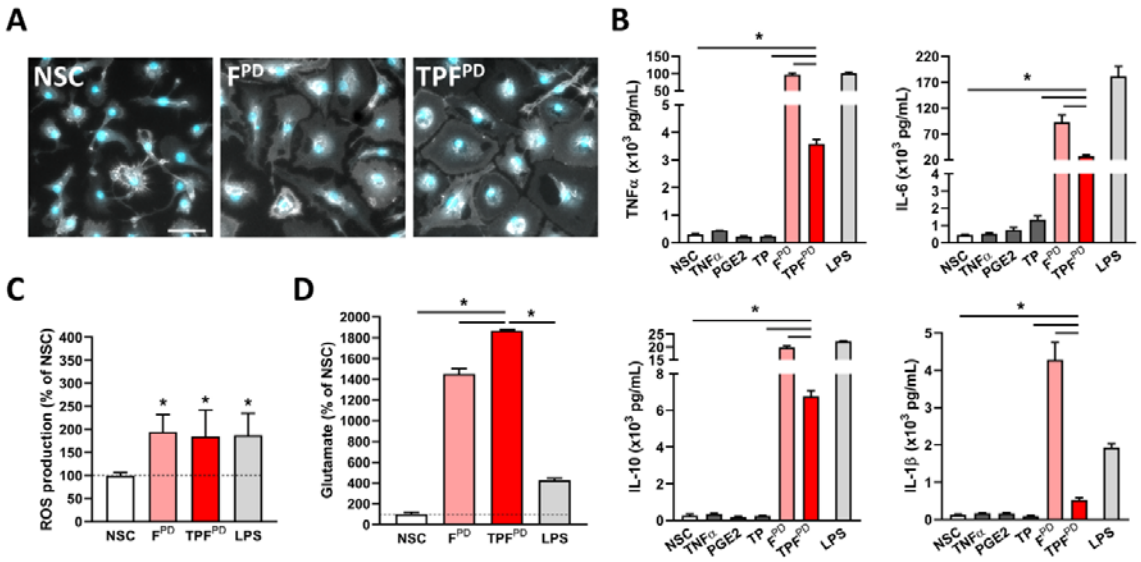

543

544 **Figure 3. TPF^{PD}-related chronic-type inflammatory stimulation of microglia is associated with lower**

545 **cytokine but increased glutamate release.** (**A**) Representative images of CD11b immunostaining and

546 Hoechst nuclear staining (blue) of microglial cells following inflammatory stimulation by PD patient-

547 derived αSYN fibrils (1.5 µM; F^{PD}) or TPF^{PD} as compared to nonstimulated cells (NSC). Note that F^{PD}

548 and TPF^{PD} induce similar morphological changes of microglial cells. Scale bar: 50µm. (**B**)

549 Quantification of TNFα, IL6, IL10 and IL1β release by microglial cells exposed or not (NSC) to TNFα

550 (800 IU/mL), PGE$_2$ (1 µg/mL), TNFα+PGE$_2$ (TP), F^{PD} (1.5 µM), TNFα+PGE$_2$+F^{PD} (TPF^{PD}) or LPS (10

551 ng/mL). The data are represented as the means±SEM (n=3-6). *p < 0.05; **p < 0.01; ***p <

552 0.001 vs. F^{S} (Student's t-test). (**C**) Quantification of ROS production measured by the NBT reaction in

553 microglial cells exposed or not (NSC) to F^{PD} (1.5 µM), TPF^{PD} or LPS (10 ng/mL). The data are expressed

554 as a % of the NSC control. The bars are the means±SEM (n=6). *p<0.05 vs. NSC (Student's t-

555 test). (**D**) Quantification of glutamate release by microglial cells exposed or not (NSC) to F^{PD} (1.5 µM),

556 TPF^{PD} or LPS (10ng/mL). The data are expressed as a % of the NSC control. The bars are the

557 means±SEM (n=3-6). *p < 0.05 vs. TPF^{PD} (Tukey's test).

558

559 **Chronic-type inflammatory stimulation of microglia is associated with a specific genomic signature.**

560 The above data showing specific inflammatory features of microglia subjected to TPF^{PD} stimulation
561 might indicate unique molecular pathway engagement and transcriptional programming as
562 previously exemplified in peripheral macrophages [21]. To elucidate the molecular signature of this
563 inflammatory polarization, we conducted unbiased transcriptomic analysis through RNA-sequencing
564 (RNA-seq) performed on nonstimulated cells (NSCs), LPS-polarized cells as a reference for the M1
565 proinflammatory state, and TPF^{PD}-activated microglia. To examine the effect of stimulation, we
566 initially performed unsupervised principal component analysis (PCA). As expected, the samples were
567 separated well by activation status (NSC vs stimulated) on the first principal component but also by
568 type of stimulation (LPS vs TPF^{PD}), which drove the second component of the variability (Fig. 4A). By
569 using differentially expressed genes (DEGs; log2FC > 0.5, false discovery rate [FDR] adjusted *P* value <
570 0.05) between TPF^{PD}, M1 (LPS) and NSCs we identified 554 upregulated and 456 downregulated
571 genes in TPF^{PD}-exposed cells. Unsupervised cluster analysis of the top 413 DEGs (by *P*-value) revealed
572 a striking difference between the transcriptomes of M1-polarized and TPF^{PD}-treated microglia (Fig.
573 4B). To obtain insights into how differential gene regulation translates into pathway modulation we
574 first processed expression data with the Pathifier algorithm, which transforms gene-level information
575 into pathway-level records [56]. Principal component analysis of the newly generated pathway-
576 related dataset indicated that both the stimulation and type of stimuli drove strong pathway
577 variability (Fig. 4C). To document in detail the pathways and biological functions altered by chronic-
578 type inflammatory stimulation, we performed pathway enrichment (KEGG) and gene ontology (GO)
579 term analyses. We found that among the most significantly enriched KEGG pathways in TPF^{PD}-
580 stimulated cells were ribosome biogenesis, glutathione metabolism, steroid biosynthesis,
581 spliceosome, ferroptosis and RNA transport (Fig. 4D). The results from GO analysis confirmed the
582 pathway enrichment data for the most part. Yet, they also revealed additional features related to the
583 regulation of the inflammatory response and primary metabolic and lipid processes (Additional File 1:
584 Fig. S2). Notably, increased glutathione metabolism in TPF^{PD}-stimulated microglial cells might be
585 possible under conditions of high cysteine supply and glutamate levels provided that the expression

586 and/or activity of the rate-limiting enzymes glutathione cysteine ligase (GCL) and glutathione
587 synthase (GSS) increase. One possible mechanism that could increase microglial cysteine levels upon
588 inflammatory stimulation is the activation of xCT, a transmembrane cystine-glutamate exchange
589 transporter encoded by the *Slc7a11* gene [57]. Remarkably, the *Slc7a11*, *Gss* and *Gcl* genes (*Gclc* and
590 *Gclm*) were among the most upregulated genes in TPF^{PD}-stimulated cells (Fig. 4E). Increased *Slc7a11*
591 gene expression in TPF^{PD}-stimulated microglia was consistent with the increased capacity of these
592 cells to release glutamate (Fig. 3C).
593 Another interesting observation is the apparent link between TPF^{PD} stimulation and ferroptosis.
594 Ferroptosis is a type of redox-driven programmed cell death process distinct from classical apoptosis.
595 This process might occur because of uncontrolled iron metabolism, lipid peroxidation and thiol
596 regulation, three processes that are commonly found in the proinflammatory environment. Since
597 TPF^{PD}-stimulation does not induce microglial cell death under our experimental conditions
598 (Additional File 1: Fig. S3), it is likely that genes involved in iron metabolism contributed to the
599 ferroptosis term in our pathway enrichment list. Indeed, we found that iron transport- and storage-
600 related genes, including *Tfrc*, *Slc39a14* and *Fth1* (encoding for the Transferrin receptor, the zinc and
601 non-transferrin-bound iron transporter Zip14, and the Ferritin heavy chain, respectively) were
602 strongly and differentially upregulated in TPF^{PD}-treated cells (Fig. 4E). The genes encoding divalent
603 metal transporter 1 (DMT1) and the iron extruder Ferroportin (*Slc11a2* and *Slc40a1*) were similarly
604 expressed in LPS- and TPF^{PD}-exposed cells (Fig. 4E). Overall, our data suggest differences in microglial
605 iron handling under two distinct inflammatory conditions.
606 To validate our transcriptomic data, we performed qPCR expression analysis of gene candidates using
607 total RNA isolated from microglial cells exposed or not to LPS and TPF^{PD} in an independent
608 experiment. We confirmed the differential expression of *Gss*, *Gclc, Gclm* and *Slc7a11* in TPF^{PD}-treated
609 cells compared to that in nonstimulated and LPS-exposed microglia (Fig. 4F). Likewise, iron
610 metabolism-related genes (*Tfrc*, *Slc39a14*, *Fth1*, *Slc11a2* and *Slc40a1*) exhibited similar changes in

611 expression as identified via transcriptomic analysis (Fig. 4F). Overall, we identified genes and

612 pathways that define microglia polarized upon TPF^{PD} chronic-type inflammatory conditions.

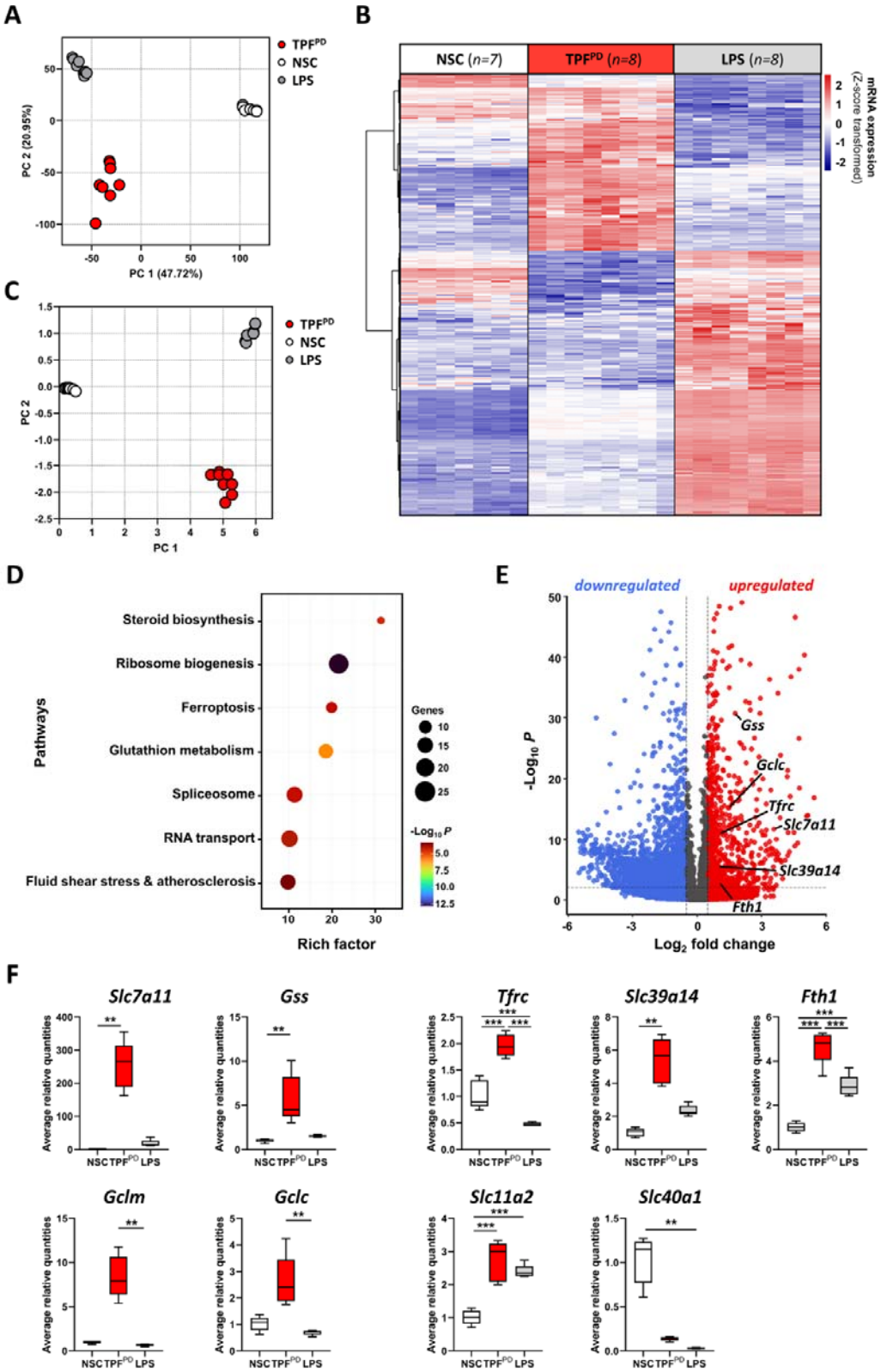

613

614 **Figure 4. Specific transcriptional reprogramming of microglial cells upon TPF^{PD} chronic-type**
615 **inflammatory activation.** (**A**) Principal component analysis (PCA) of gene expression data based on
616 the first two PCs shows, on the one hand, a clear distinction between nonstimulated (NSC) and
617 activated cells (LPS and TPF^{PD}) and, on the other hand, strong differences between M1-type (LPS) and
618 chronic-type (TPF^{PD}) inflammatory activation. (**B**) Hierarchical clustering and heatmap of differentially
619 expressed genes (DEGs; n=413) in TPF^{PD}-activated microglia versus nonstimulated (NSC) and LPS-
620 treated cells. The scaled expression value (Z-score transformed) is shown in a blue-red color scheme
621 with red indicating higher expression, and blue lower expression. Biological replicates are indicated
622 in brackets. (**C**) PCA analysis of pathway-related data generated by the Pathifier method (Drier et al.,
623 2013) demonstrates clear clustering and separation of stimulated and nonstimulated (NSC) cells and
624 of M1-type (LPS) and chronic-type (TPF^{PD}) inflammatory activation. (**D**) Bubble chart showing the
625 enrichment of the KEGG Pathway in TPF^{PD}-treated microglial cells (adjusted $p < 0.05$). The bubble size
626 indicates the number of genes annotated in the indicated KEGG pathway. The colors represent
627 pathway enrichment (% of overlapping genes) in TPF^{PD}-exposed cells. (**E**) Volcano plot depicting
628 individual DEGs ($|\text{Log}_2 \text{ Fold Change}| > 2$) in TPF^{PD}-treated microglia versus M1-type (LPS) activated
629 cells. The red and blue dots show upregulated and downregulated genes in TPF^{PD}-treated cells,
630 respectively. Individual genes of interest are indicated. (**F**) Relative gene expression analysis (qPCR) of
631 individual gene candidates in nonstimulated- (NSC), LPS-activated and TPF^{PD}-exposed microglial cells.
632 The data are represented as the means ± SEM (n=5 biological replicates from independent
633 experiment). $*p < 0.05$ vs TPF^{PD} (Student's t test).
634
635
636 **TPF^{PD}-related chronic-type inflammatory stimulation of microglia is associated with M1-related**
637 **metabolic changes.**
638 The above transcriptome-based analysis revealed pathway enrichment linked to metabolic
639 processes. It is now well established that immune activation rapidly and substantially enhances

640 metabolic outputs that in turn regulate immune responses [58]. For instance, in macrophages,
641 including microglia, M1 phenotype polarization is accompanied by a shift from oxidative
642 phosphorylation to aerobic glycolysis for energy production [59]. To further investigate TPF^{PD}-
643 associated metabolic changes in microglia, we performed untargeted metabolomic analysis under
644 the same experimental conditions as above.

645 Our results revealed significant alterations in the levels of 248 metabolites in TPF^{PD}-treated cells.
646 Indeed, hierarchical clustering analysis of metabolite datasets and heatmap generation (Fig. 5A)
647 showed important differences between nonstimulated cells and microglia exposed to either LPS or
648 TPF^{PD}. The metabolome profile of TPF^{PD}-activated cells displayed only subtle differences from that of
649 LPS-treated microglia. Of the 248 metabolites showing significant changes, only 28 were annotated in
650 the databases. Unsupervised cluster analysis of these 28 known metabolites confirmed the close
651 relationship between the two inflammatory conditions (Fig. 5B). In particular, both stimulations
652 resulted in decreased α-ketoglutarate/succinate and fumarate/succinate ratios, which are indicative
653 of tricarboxylic acid (TCA) cycle breaks and metabolic switches from oxidative phosphorylation to
654 glycolysis, as previously reported [60]. Hence, these data suggest that from a respiratory point of
655 view, TPF^{PD}-polarized microglia behave as classical proinflammatory M1 cells. Moreover, although
656 TPF^{PD}-polarized microglia release more glutamate than LPS-activated cells (Fig. 3C), these two
657 inflammatory stimulations are characterized by comparable increases in glutamate and glutathione
658 disulfide levels (Fig. 5C). Hence, our data showed that metabolic changes associated with M1 and
659 TPF^{PD} microglial polarization are closely related.

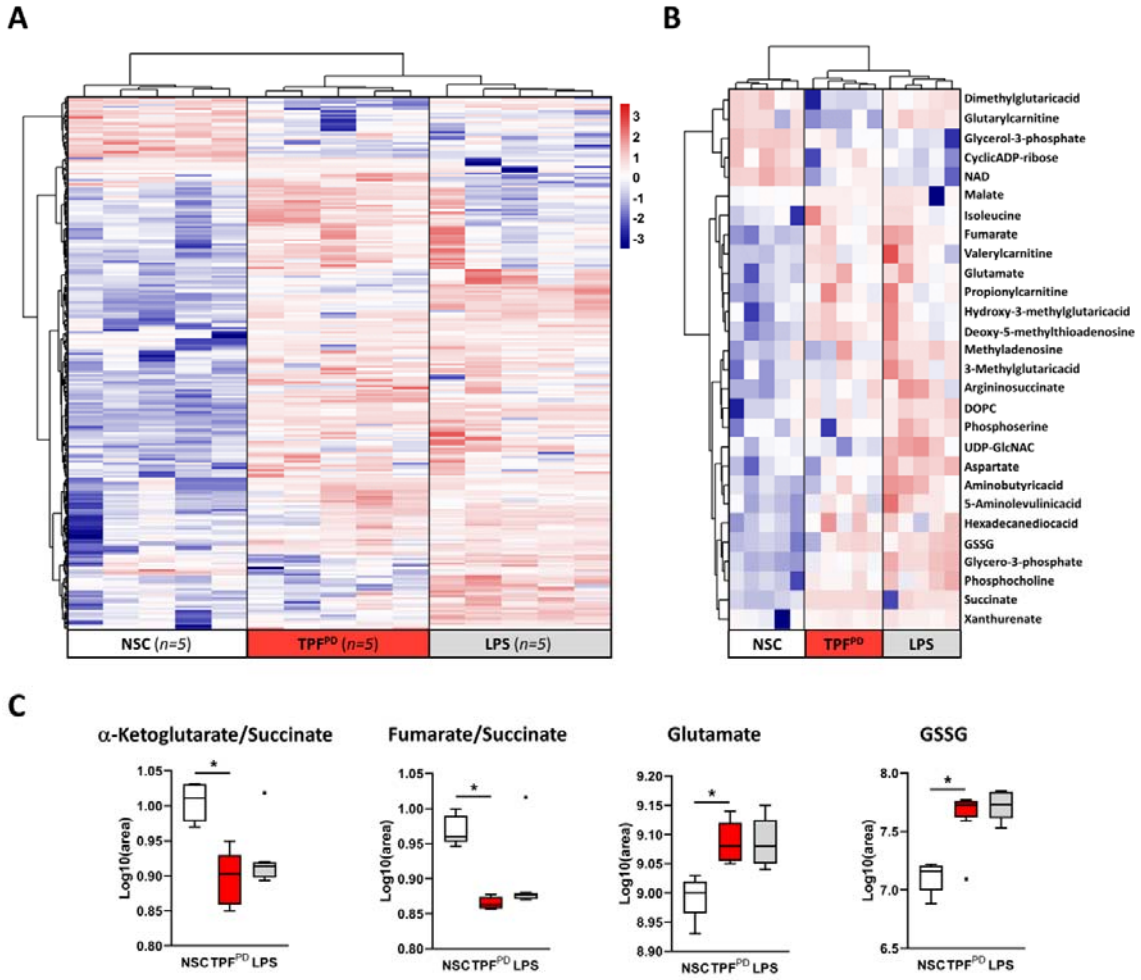

Figure 5. Microglial metabolic reprogramming evoked by TPF^{PD} is closely related to M1-type polarized cells. (**A**) Hierarchical clustering analysis and heatmap visualization of 248 differentially regulated metabolites (28 annotated and 220 unknown/nonannotated metabolites) in stimulated cells (LPS and TPF^{PD}) compared to those in the NSC control group. The number of biological replicates is indicated in brackets. Clear changes in the metabolic profile between stimulated and nonstimulated cells are observed. (**B**) Hierarchical clustering analysis and heatmap visualization of the 28 annotated metabolites extracted from (A). Despite these subtle differences, the TPF^{PD}- and LPS-associated metabolic signatures are closely related. (**C**) Box plots showing the relative amount of a-ketoglutarate, succinate, fumarate, glutamate and glutathione disulfide (GSSG) in control (NSC) and in LPS- and TPF^{PD}-treated microglial cells. Similar decreases in the a-ketoglutarate/succinate and fumarate/succinate ratios were found in LPS- and TPF^{PD}-stimulated cells. Likewise, similar increases

672 in glutamate and GSSG levels were observed under both stimulatory conditions. *$p < 0.05$ (Kruskal-
673 Wallis & Wilcoxon test).
674
675 **Conserved TPF^{PD}-specific induction of Tfrc and Slc7a11 gene expression in human induced**
676 **microglial-like cells.**
677 Integration and comparison of human and murine transcriptome datasets indicate both divergent
678 and conserved gene expression regulation upon inflammatory stimulation between species [61]. Our
679 comparative study of TPP-induced inflammatory markers in mouse microglial cells clearly illustrates
680 such divergence indicating cell-type and/or species specificity (Fig. 2). To further determine the
681 relevance of our data generated from mouse microglia, we prepared and used induced-microglia-like
682 cells (iMGs) differentiated from human monocytes isolated from healthy donors [48]. Successful
683 differentiation of monocytes into iMGs was confirmed by investigating the expression of the CCR2
684 and CX3CR1 chemokine receptors. As shown in Figure 6A, monocyte differentiation into iMGs was
685 accompanied by a significant increase in the CX3CR1/CCR2 ratio indicating that differentiated cells
686 acquired a macrophage-/microglia-like phenotype [60]. After 24 days of differentiation, iMGs were
687 exposed or not (NSC) to LPS, F^{PD} or TPF^{PD} at concentrations equivalent to those used for mouse
688 microglia experiments and then collected after 48 hours of activation for assessment by qPCR of
689 candidate genes. We found that, similar to mouse microglial cells, TPF^{PD} chronic-type inflammatory
690 stimulation of iMGs resulted in specific upregulation of *Tfrc* and *Slc7a11* compared to that in
691 response to LPS or F^{PD} treatment (Fig. 6B). Likewise, although not significantly different, a clear trend
692 toward increased expression of *Slc11a2* was observed under both LPS and TPF^{PD} conditions. In
693 contrast, *Gclm* was found to be equally induced in LPS- and TPF^{PD}-exposed cells but not in cells
694 stimulated with F^{PD} alone. Interestingly, compared with LPS and F^{PD}, TPF^{PD} stimulation specifically
695 induced marked upregulation of *Tlr2* in iMGs in contrast to what we observed in mouse microglial
696 cells. Moreover, while *Tlr4* expression was reduced upon LPS and F^{PD} treatment compared to that in
697 control cells (NSC), it remained unchanged under TPF^{PD} conditions suggesting that the regulation of

698 TLR expression in human microglia highly depends on the type of inflammation and inflammatory
699 stimuli. Together, our data support previous findings showing species-dependent gene regulation in
700 macrophages and demonstrate conserved TPF^{PD}-associated *Tfrc* and *Slc7a11* gene regulation
701 between mouse and human microglia. They further highlight that TPF^{PD}-stimulated microglia may
702 acquire a unique phenotype characterized by increased iron retention capacity and glutamate
703 release.

704

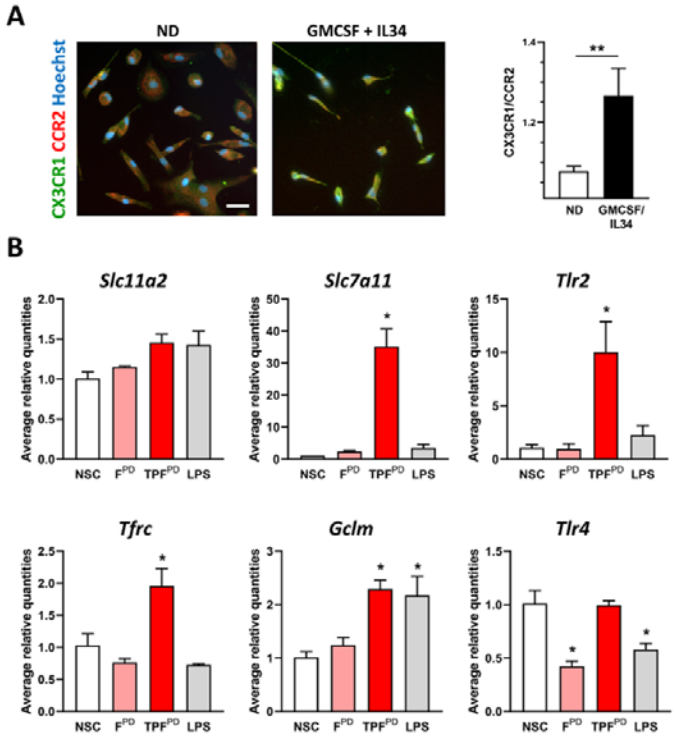

705

706 **Figure 6. Compared with mouse microglia, TPF^{PD}-exposed human microglial-like cells exhibit both**
707 **conserved and distinct gene regulation.** (**A**) Representative images showing CCR2 (red) and CX3CR1
708 (green) double immunostaining with Hoechst nuclear stain (blue) in nondifferentiated (ND) and GM-
709 CSF/IL34-differentiated human monocytes (iMG) after 16 days of culture. The right panel shows the
710 quantification of the immunosignal CX3CR1/CRR2 ratio in ND and GM-CSF/IL34-differentiated cells.
711 The data are presented as the means ± SEM (n = 4-5). ** p < 0.01 vs. ND (Student's t-test). Scale
712 bar: 40 µm (**B**) Relative expression analysis (qPCR) of individual gene candidates in nonstimulated

713 (NSC), LPS-, F^{PD}- and TPF^{PD}-activated iMGs. The data are presented as the means ± SEM (biological
714 replicates n=3). *$p < 0.05$ vs. TPF^{PD} (Student's t test).

715 **Chronic-type inflammatory stimulation of microglia results in xCT-dependent neurotoxicity on**
716 **dopaminergic neurons.**

717 Our molecular and phenotypic analysis of microglial cells stimulated by chronic-type inflammatory
718 cues revealed that cells under such activation are more prone to release high amounts of glutamate
719 than classically activated (M1) proinflammatory microglia. This peculiar effector function of TPF^{PD}-
720 activated cells may be detrimental to dopaminergic neurons, which are particularly vulnerable to
721 glutamate-induced excitotoxicity [63]. We sought to test this hypothesis using an experimental
722 paradigm, allowing us to evaluate the neurotoxic potential of microglia-conditioned medium (MCM)
723 on dopaminergic neurons. Specifically, we tested and compared the survival of dopaminergic
724 neurons maintained in Nb^{S}-based ACM, 24 hours after they received MCM (30%, v/v) from F^{PD}- and
725 TPF^{PD}-stimulated microglia cultivated in $DMEM^{S}$-based ACM (Fig. 7A). To prevent any possible direct
726 neuronal effects of inflammatory stimulating factors (F^{PD} or TPF^{PD}), we implemented a washout step
727 6 h after initiating microglial stimulation and maintained activated microglial cells for an additional
728 24 hours in fresh $DMEM^{S}$-based ACM (Fig. 7A). At this time, MCM from F^{PD}- or TPF^{PD}-stimulated
729 microglia displayed higher glutamate levels than did those from NSC (Fig. 7B). Under such
730 experimental setup, we found that TPF^{PD}-stimulated MCM induced significantly more TH+
731 dopaminergic neuron loss than did F^{PD}-stimulated cells suggesting that chronic-type inflammatory
732 stimulation drives microglia toward a more aggressive phenotype than classically activated M1 cells
733 (Fig. 7C and D). Most interestingly, we observed that the rate of TH+ neuronal loss was strongly
734 correlated with the glutamate content in the MCM suggesting that xCT-dependent glutamate release
735 and glutamate-induced excitotoxicity may underlie key neurotoxic mechanisms supported by
736 chronic-type inflammatory microglial cells (Fig. 7E). Importantly, the transfer of $DMEM^{S}$-based ACM
737 from control microglial cultures to midbrain cells had no impact on dopaminergic neuron survival.

738 To further strengthen our hypothesis, we exposed F^{PD}- and TPF^{PD}-stimulated microglial cells to the
739 xCT inhibitor Sulfasalazine (250 µM) during the 24 hour of the washout step and subsequently
740 transferred the resulting MCM onto midbrain neurons. Sulfasalazine treatment of stimulated
741 microglial cells completely abrogated MCM-associated dopaminergic toxicity, suggesting an essential
742 role of xCT in the neurotoxic activity of chronic-type inflammatory microglial cells (Fig. 7D). Finally, to
743 establish that TPF^{PD}-activated microglial cells induce dopaminergic cell death through glutamate-
744 dependent excitotoxic mechanisms, we treated MCM-exposed midbrain cultures with MK-801 (2
745 µM), an inhibitor of the glutamate receptor *N*-methyl-D-aspartate receptor (NMDAR). As shown in
746 Figure 7D, MK-801 treatment fully protected against MCM-associated damage, indicating that
747 chronic-type inflammatory microglial cells promote dopaminergic neuronal death by excitotoxicity.
748

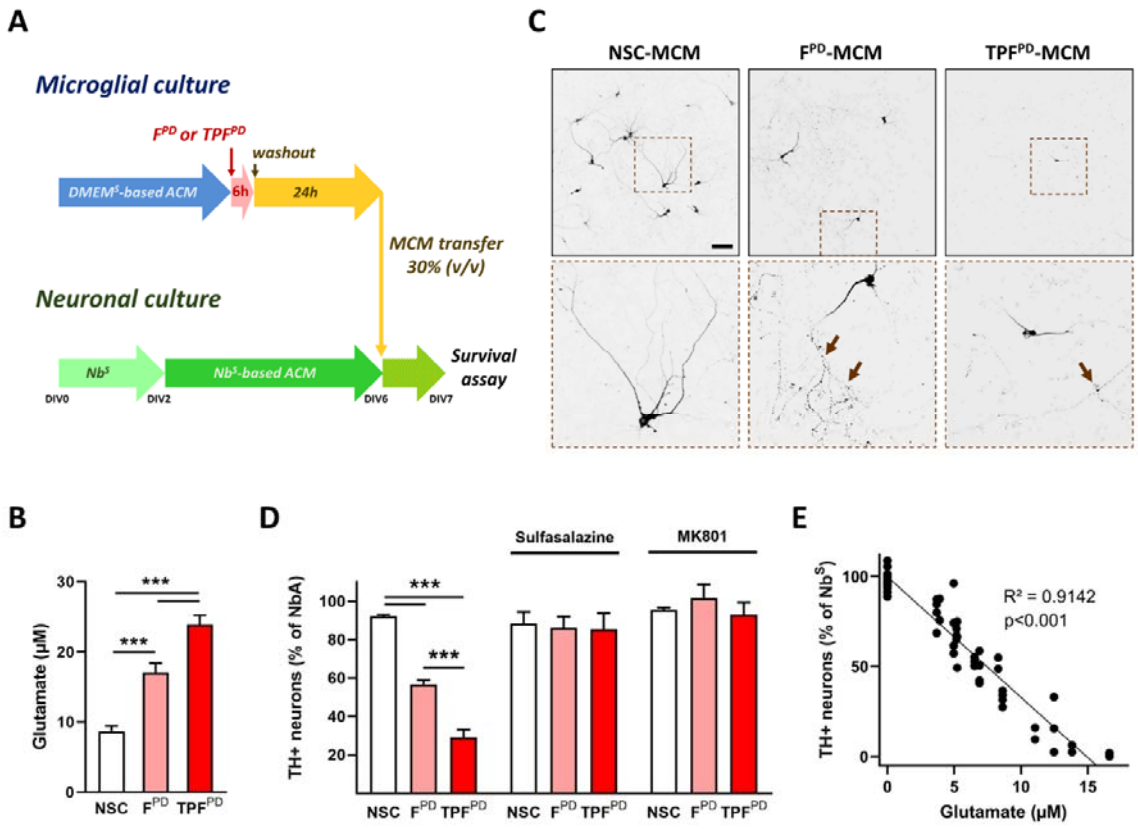

749

750 **Figure 7. TPF^{PD}-stimulated microglial cells trigger more excitotoxic cell death than F^{PD}-exposed cells**
751 **on dopaminergic neurons.** (**A**) Schematic representation of the experimental setup used to analyze

752 the neurotoxic potential of chronic-type inflammatory microglia. Microglial cell cultures were
753 maintained in DMEM^{S}-based astrocyte-conditioned medium (ACM) and exposed or not (NSC) for 6
754 hours to either F^{PD} or TPF^{PD}. Following inflammatory stimulation, the culture medium was fully
755 replaced with fresh DMEM^{S}-based ACM (washout step), and the microglial cells were left for 24
756 hours before the glutamate assay (**B**). Midbrain neuronal cultures were prepared from E13.5 mouse
757 embryos and maintained for 2 days in Nb^{S}. On day *in vitro* 2 (DIV2), the culture medium was fully
758 replaced with Nb^{S}-based ACM and the neurons were left to mature until DIV6. At DIV6, 30% (v/v) of
759 the Nb^{S}-based ACM media was replaced with microglia-conditioned media (MCM) and TH+
760 dopaminergic neuron survival was assayed 24 hours later. The data are presented as the
761 means ± SEM (biological replicates n=13; 3 independent experiments). ***$p < 0.001$ vs NSC and F^{PD}
762 (One-way ANOVA followed by Tukey's test). (**C**) Low- and high-magnification (dashed brown squares)
763 images of DIV7 midbrain cultures exposed for 24 hours to MCM from F^{PD} and TPF^{PD}-stimulated or
764 unstimulated cells (NSC). Brown arrows point to dystrophic cell bodies and processes with
765 varicosities. Scale Bar = 100 µm. (**D**) Survival of TH+ neurons in DIV7 midbrain cultures exposed for 24
766 hours to MCM from F^{PD} and TPF^{PD}-stimulated or unstimulated cells (NSC). In sister cultures, neurons
767 were exposed to MCM from F^{PD} and TPF^{PD}-stimulated microglial cells treated with the xCT inhibitor
768 Sulfasalazine (250 µM) during the 24 hours washout period. In additional sister cultures, neurons
769 exposed to MCM from F^{PD} and TPF^{PD}-stimulated microglial cells were cotreated with the *N*-methyl-D-
770 aspartate (NMDA) receptor pore blocker MK-801 (2 µM). The data are presented as the means ± SEM
771 (biological replicates n=5-8; 2 independent experiments). *** $p < 0.001$ vs. NSC or F^{PD} (One-way
772 ANOVA followed by pairwise multiple comparisons using the Holm-Sidak method). (**E**) TH+
773 dopaminergic neuron survival is inversely correlated with the concentration of glutamate within the
774 transferred MCM (linear regression analysis).
775
776 **Discussion**

777 In this study, we investigated the inflammatory properties of PD patient-derived αSYN fibrils on
778 microglial cells and explored their capacity to induce a unique immune response when combined
779 with TNFα and prostaglandin E_2 (PGE_2), two inflammatory cues commonly elevated in chronic
780 inflammatory diseases and in PD patients. We found that fibrils derived from the PMCA of PD patient
781 tissue have stronger inflammatory potency than recombinant human αSYN fibrils generated *de novo*
782 in cultured mouse microglia suggesting a relationship between the structure of aggregated αSYN and
783 the macrophage immune response. Importantly, the inflammatory response elicited by PD patient-
784 derived αSYN fibrils on microglia was profoundly modulated in the presence of TNFα and PGE_2 with
785 lower cytokine but higher glutamate release responsiveness. This "chronic-type" inflammatory
786 stimulation results in specific molecular reprogramming of microglial cells that depart from classically
787 activated and proinflammatory M1 microglia and is characterized by seemingly increased iron
788 retention and excitotoxic capacities.
789 Microglia, the most abundant resident macrophages of the central nervous system (CNS), play
790 important roles in the maintenance of tissue homeostasis [64-66]. However, upon neuronal injury,
791 microglia are rapidly activated and mount an inflammatory response that, if persistent, can prove
792 neurotoxic [67-69]. In PD, protracted microglial cell activation is a neuropathological characteristic
793 that accompanies neurodegeneration and deposition of pathological αSYN [70]. Protein aggregates
794 are common features of several age-related neurodegenerative diseases and have been linked to
795 microglial cell activation and the ensuing inflammatory response through ligation of pattern
796 recognition receptors (PRRs) [5]. Mounting evidence suggests that αSYN aggregates, which are
797 eventually released from neurons as part of the prion-like propagation mechanism of the
798 synucleinopathies across neuronal networks, are a major pathological trigger of microglial activation
799 and inflammation in PD [52, 71]. Yet, the importance of the respective PRRs in this process is still a
800 subject of debate. While some authors have noted a key role for TLR2, others have found that TLR4
801 may also be important [53, 72-74]. The discrepancy between these results is likely to stem from the
802 type and purity of the αSYN assemblies used in different studies. Recently, using distinct well-

803 characterized recombinant human αSYN assemblies generated *de novo*, we found that TLR2 and
804 TLR5, but not TLR4, were indispensable for monomeric and oligomeric αSYN to efficiently activate
805 the NOD-like receptor pyrin domain containing 3 (NLRP3) inflammasome and IL1β release from
806 microglial cells [8]. Equal concentrations of αSYN fibrillar polymorphs were unable to evoke IL1β
807 release during the same stimulation period [8]. Thus, these data strongly suggest that the structural
808 characteristics of αSYN assemblies are major determinants of their innate immunological properties.
809 In support of this view, we showed here that fibrils derived from PD patients (F^{PD}) elicited a greater
810 inflammatory response than fibrils assembled *de novo* but a lower response than fibrils amplified
811 from DLB patients (F^{DLB}). Strikingly, whereas F^{S} (2 μM) was unable to induce IL1β release in unprimed
812 microglial cells [8], we found that lower concentrations of F^{PD} (1.5 μM) induced a robust IL1β
813 response (Fig. 3B). Since F^{PD} are structurally different from F^{DLB} and F^{S} [75, 76], our data further
814 support the view that αSYN assemblies with different structures have distinct inflammatory potency
815 on microglial cells. The structure-function relationship depicted here for the microglia-associated
816 immune response is reminiscent of that documented for neuronal deposition of pathological αSYN
817 and toxicity [15, 77]. Indeed, we recently reported that structurally distinct αSYN fibrils assembled *de*
818 *novo* or derived from PD, DLB and MSA patients result in different synucleinopathy-associated
819 characteristics and toxicity in cultured cells and after inoculation in rodent brains [12, 14, 15]. The
820 different biological properties between patient-derived and *de novo* assembled fibrils may originate
821 from the different surfaces that distinct fibrillar polymorphs expose to the solvent which define their
822 differential binding to cell surface proteins, seeding propensity in cells and turnover [12, 16]. Hence,
823 it is likely that the capacity of the F^{PD} polymorph to evoke a stronger inflammatory response than its
824 recombinant counterpart might be linked to its ability to bind with higher affinity to innate immune
825 receptors or to activate different types of receptors. However, the binding capacity of F^{PD} to different
826 TLRs or other innate immune receptors has yet to be established.
827 A major contribution of our study is the demonstration that the F^{PD}-induced microglial inflammatory
828 response is profoundly altered when associated with the proinflammatory cytokine TNFα and PGE_2,

829 an arachidonic acid-derived lipid modulator of inflammation. As part of this study, we further showed
830 that under such combinatory stimulation (so called TPF^{PD}), microglial cells engage a distinct molecular
831 program from that of LPS-induced proinflammatory M1 cells. TNFα and PGE_2, are common immune-
832 related factors featuring chronic inflammatory conditions [78, 79]. In PD, a neurodegenerative
833 disease associated with chronic neuroinflammatory processes, the expression level of TNFα and the
834 PGE_2-producing enzyme cyclooxygenase 2 (COX2) were shown to increase [80-82]. Moreover,
835 compelling experimental evidence supports an independent pathogenic role of these inflammatory
836 factors, suggesting that in addition to being part of a large panel of effector molecules derived from
837 activated glial cells or injured neurons, these inflammatory cues are instrumental in neuronal cell
838 death [83, 84]. Hence, although αSYN aggregates are considered primary and master disease-
839 associated inflammatory triggers in PD, other immune-related factors, as part of a global network of
840 neuroinflammatory processes [4], may significantly contribute to regulating microglia-associated
841 inflammation and toxicity. Indeed, it is now well established that microglial cells, and tissue
842 macrophages in general, are very plastic and can adopt a wide variety of activation phenotypes
843 associated with specific functions. Analysis and network modeling of transcriptional regulation during
844 human macrophage activation elicited by a diverse set of stimuli have clearly established a spectrum
845 model of macrophage activation that reassesses and extends the prevailing M1 (proinflammatory or
846 classically activated) versus M2 (anti-inflammatory or alternatively activated) polarization model
847 [21]. Notably, macrophages exposed to the combination of chronic inflammation-associated factor
848 TNFα, PGE_2, and TLR2 ligands (the so-called "TPP" stimulation) feature specific molecular modules
849 not found in IFNγ- (M1) or IL4- (M2) stimulated cells and consequently express specific cell surface
850 markers and cytokines. However, the findings obtained in human macrophages might not be
851 generalizable to murine microglia. Indeed, we found that the regulation of TPP-specific markers
852 (CD25, CXCL5 and IL1α) in mouse microglial cells was markedly different from that in human
853 macrophages highlighting important macrophage identity- and/or species-related specificity, as
854 previously reviewed [85]. Yet, despite these differences, our results clearly show that, as

855 documented in human macrophages, chronic-type inflammatory stimulation of microglia is
856 associated with specific transcriptional reprogramming departing from classically activated M1 cells.
857 Interestingly, some of the molecular pathways characterizing chronic-type inflammatory stimulation
858 were consistent with previously defined functional properties. In particular, the finding that TPF^{PD}-
859 stimulated cells feature higher xCT-encoding *Slc7a11* gene expression is consistent with the
860 enhanced responsiveness of these cells to glutamate release. Importantly, a similar upregulation of
861 *Slc7a11* was detected in human microglial-like cells (iMGs) exposed to TPF^{PD} arguing that this
862 chronic-type inflammatory-associated regulation is conserved across mouse and human species.
863 While releasing glutamate, the xCT antiporter internalizes cystine, which is needed for glutathione
864 synthesis. In line with this scenario, we further observed that TPF^{PD}-polarized microglial cells are
865 characterized by the specific upregulation of several genes (*Gss, Gclc* and *Gclm*) encoding rate-
866 limiting enzymes involved in glutathione synthesis. The cystine-glutamate antiporter xCT has been
867 previously shown to contribute to the proinflammatory phenotype of primary microglial cells and to
868 be involved in amyotrophic lateral sclerosis (ALS)- and Alzheimer's disease-related pathogenesis [86,
869 87]. In particular, decreased production of specific microglial proinflammatory/neurotoxic factors
870 including nitric oxide, TNFα and IL6 was observed in xCT-deleted microglial cells exposed to LPS [86].
871 Our data showing decreased TNFα and IL6 production concomitant with increased *Slc7a11* gene
872 expression and glutamate release in TPF^{PD}-stimulated microglia suggest that the regulatory
873 mechanisms of proinflammatory cytokine expression induced by xCT differ between different
874 microglial activation states. Hence, the importance of our finding in the context of PD-related
875 neuroinflammation stems from the fact that glutamate has the potential to generate low-level
876 excitotoxic insults [88] that may contribute to neuronal cell death [89]. In line with this, we provide
877 compelling evidence that xCT-dependent glutamate release from chronic-type inflammatory
878 microglia results in NMDAR overactivation-mediated excitotoxic dopaminergic cell death. In the field
879 of PD, previous studies have reported an increase in xCT expression upon injection of 6-
880 hydroxydopamine (6-OHDA) in hemi-Parkinson rats [90]. Moreover, neuroprotection has been

881 documented in xCT-null mice injected with 6-OHDA [91]. Yet, inhibition of xCT by genetic targeting
882 does not protect mice from MPTP-induced dopaminergic cell loss [92]. Thus, although debated, the
883 role of xCT in PD pathogenesis is still unclear. Notably, its pathogenic role has never been
884 investigated in PD animal models featuring degenerative synucleinopathy.
885 Apart from glutathione metabolism, the identification of the TPF^{PD}-specific ferroptotic pathway in our
886 KEGG analysis was surprising given the fact that we did not observe microglial cell death upon
887 exposure to TPF^{PD}. It has been documented that macrophages display significant defiance against
888 ferroptotic stimulation and death, particularly when polarized into classically activated M1 state [93].
889 Yet, as part of the set of genes involved in this pathway, TPF^{PD} stimulation was associated with
890 elevated expression of iron-related transport proteins coupled with increased intracellular iron-
891 storage capacity. Increased iron retention is a well-known function of inflammatory macrophages
892 that serves as a primary defense mechanism against pathogens through extracellular iron starvation.
893 Yet, macrophage iron uptake fulfills additional important role as it is an essential metal that fine-
894 tunes metabolic changes associated with immune activation thereby contributing directly to
895 macrophage function and plasticity [94]. A previous report indicated that M1-type microglia
896 preferentially acquire iron from non-Transferrin-bound iron (NTBI), whereas M2 polarized cells
897 promote TBI uptake [95]. Our data are consistent with this general scheme since LPS-induced
898 microglial activation was associated with concomitant increases and decreases in the gene
899 expression of *Slc11a2* (encoding divalent metal transporter 1; DMT1) and *Tfrc* (encoding the
900 Transferrin receptor), respectively. Remarkably, however, TPF^{PD}-stimulated cells were characterized
901 by increased gene expression of both *Slc11a2* and *Tfrc*, indicating a unique iron transport phenotype
902 featuring both M1 and M2 properties. The presumably greater iron retention capacity of TPF^{PD}-
903 stimulated cells than of LPS-polarized microglia is further supported by the specific upregulation of
904 the gene encoding for ZIP14 (*Slc39a14*), a complex broad-scope metal-ion transporter of zinc and
905 non-transferrin-bound iron. Coupled with increased iron uptake capacity, TPF^{PD}-polarized microglia
906 further displayed a high decrease in *Slc40a1* gene expression (encoding the iron extruder

907 Ferroportin) as well as a robust increase in *Fth1*, which encodes the iron storage Ferritin heavy chain.
908 As for *Slc7a11* gene regulation, TPF^{PD}-elicited *Tfrc* and *Slc11a2* upregulated gene expression was
909 conserved in human iMGs confirming the relevance of our findings in humans. Taken together, these
910 data suggest that microglial cells polarized under TPF^{PD}-associated chronic-type inflammation feature
911 both M1- and M2-associated iron metabolism regulation and propose that they might be particularly
912 iron retentive compared to M1 and M2 inflammatory cells. Relevant to our findings, is the
913 observation that iron accumulates prematurely and preferentially in microglial cells rather than
914 dopaminergic neurons in a nonhuman primate model of degenerative synucleinopathy induced by
915 intranasal administration of human αSYN preformed fibrils (PFFs) [96]. Interestingly, recent data
916 obtained from a model of human induced pluripotent stem cell-derived microglia grown in a tri-
917 culture system with neurons and astrocytes have shown that iron-loaded microglial cells not only are
918 susceptible to ferroptotic cell death but also prone to inducing neuronal toxicity through a
919 mechanism that has yet to be determined [95]. Strikingly, single-cell transcriptomic and KEGG
920 pathway analyses in this model system demonstrated that ferroptosis and glutathione metabolism
921 were among the pathways most affected in microglial cells exposed to ferroptotic conditions [97].
922 These features are reminiscent of our data obtained in TPF^{PD}-stimulated primary microglial cells
923 suggesting that chronic-type inflammatory stimulation results in a microglial phenotypic shift toward
924 a strong iron-retentive state, which may eventually favor their ferroptotic death and neurotoxicity.
925 Alternatively, microglial iron loading could induce oxidative stress while decreasing their phagocytic
926 activity and release capacity of inflammatory mediators [98]. Altogether these data suggest that
927 chronic-type inflammatory microglia hold a particularly aggressive phenotype characterized by both
928 increased toxicity and loss of protective/healing properties.
929 It is now well established that in response to environmental cues, such as inflammatory stimuli,
930 microglia shift their metabolism as part of an adaptative mechanism that drives specific effector
931 functions. Notably, TLR-related proinflammatory stimulation (e.g., LPS) induces a metabolic shift
932 from oxidative phosphorylation to glycolysis, a phenomenon known as the Warburg effect initially

933 characterized in tumor cells [59, 99]. Consistent with this, we found that LPS stimulation of microglia
934 resulted in a decreased α-ketoglutarate/succinate and fumarate/succinate ratios, which are
935 indicative of tricarboxylic acid (TCA) cycle breaks. Importantly, the immune response evoked by TPF^{PD}
936 stimulation was associated with similar metabolic changes suggesting that from a respiratory point of
937 view this chronic-type inflammation shares common features with classical M1-polarized cells.
938 Surprisingly, even though TPF^{PD}-stimulated cells release more glutamate than LPS-exposed cells, we
939 observed similar intracellular levels of glutamate under these two inflammatory conditions.
940 Therefore, we posit that the greater capacity of TPF^{PD}-polarized cells to extrude glutamate is likely
941 linked to increased expression of xCT rather than enhanced glutamate synthesis pathway activity.
942 In summary, we documented that PD patient-derived αSYN fibrils hold robust inflammatory
943 properties on microglial cells. Furthermore, we showed that when combined with TNFα and PGE_2,
944 this disease-associated αSYN polymorph polarizes microglia into a specific "chronic-type"
945 inflammatory activation state and phenotype featuring both M1- and M2-related traits and
946 exhibiting overwhelming neurotoxic activities. Of note, composed M1/M2 polarization assignment
947 has been previously documented in animal models of traumatic brain injury, ALS and glioma-
948 associated neurological disease suggesting that our model system may, in part, recapitulate more
949 closely some of the complex innate inflammatory mechanisms *in vivo* [20, 100-102]. In support of
950 this view, we identified few overlaps between TPF^{PD}-stimulated microglia *in vitro* and the recently
951 characterized disease-associated microglia (DAM) isolated from mouse models of Alzheimer's
952 disease and ALS [103]. In particular, few of the genes assigned to DAMs, including B2m, Lyz2 and
953 Cst7, were found to be differentially expressed in TPF^{PD}-polarized microglia (data not shown).
954 Nonetheless, the global gene expression overlaps between the DAM transcriptome and that of LPS-
955 or TPF^{PD}-derived cells was modest (53 and 50 genes, respectively), highlighting significant differences
956 in genomic expression patterns between *in vitro* and *in vivo* microglia cells, as previously reported
957 [104]. Yet, although we are well aware that the model described here is not a phenocopy of activated
958 microglial cells in the brains of PD patients, it may serve as a general framework for exploring and

959 understanding the disease-associated mechanisms underlying complex inflammatory-induced signal
960 integration that shape microglial cell activation and function. Hence, such knowledge should facilitate
961 the identification of new potential therapeutic targets and may lead to the discovery of biomarkers.
962
963 **Ethics approval and consent to participate**
964 The protocol used for collecting human peripheral blood mononuclear cells was approved by an
965 ethical committee affiliated with French regulation authorities (CCPPRB Groupe Hospitalier Pitié-
966 Salpêtrière, Paris, France). Blood samples were collected from a donor who provided signed
967 informed consent and who was included in an INSERM-sponsored clinical study. Experimental
968 procedures in mice were authorized by the Committee on the Ethics of Animal Experiments Charles
969 Darwin N°5 under the registration number Ce5/2017/005.
970
971 **Consent for publication**
972 Not applicable.
973
974 **Availability of data and materials**
975 The datasets supporting the conclusions of this article are included within the article and its
976 additional file.
977
978 **Competing interests**
979 The authors declare that there are no conflicts of interest regarding the experimental part of this
980 study.
981 **Funding**
982 This work was supported by funding from the Joint Program on Neurodegenerative Diseases (JPND)
983 to S.H. and R.M. (01ED1603). S.H. received further funding from the Sanofi Innovation Awards -
984 Europe Program Funding Award (2018 iAward). C.Y. and P.B. were supported by the Neuroscience

School of Paris Foundation (ENP), the French Ministry of Higher Education and Research and the Association France Parkinson, respectively. The research leading to these results has received funding from the program "Investissements d'Avenir" ANR-10-IAIHU-06 and ANR-11-INBS-0011-NeurATRIS: Translational Research Infrastructure for Biotherapies in Neurosciences.

Authors' contributions

C.Y. and S.H. designed all the experiments; C.Y., L.G., J.S.-D. and P.B. performed the experiments and analyzed the data with the assistance of P.P.M. and S.H.; A.F. and R.M. generated and characterized all the α-Synuclein assemblies and provided advice; and C.Y. and S.H. wrote the manuscript with input from all the coauthors.

Acknowledgements

The authors would like to thank Prof. Jean-Christophe Corvol and the Clinical Investigation Center for Neurosciences of the Pitié-Salpêtrière Hospital (CIC 1421, Paris, France) for their help in collecting human blood samples. We are indebted to Prof. Steve Gentleman at the Neuropathology Unit, Division of Brain Sciences, Department of Medicine, Imperial College London for providing us with PD and DLB patient brain tissues. We also thank Dr. Luc Bousset for his invaluable advice in preparing αSyn assemblies *in vitro*. Part of this work was carried out on the CELIS cell culture, the iGenSeq and the Data and Analysis core facilities of ICM. We gratefully acknowledge Yannick Marie, Justine Guegan and David Akbar for helpful discussions and advice on the technical aspects of the project. We would also like to thank Farid Ichou and Maha Ponnaiah from the ICANalytics core facility (ICAN Institute, Salpêtrière Hospital, Paris France) for their help in sample preparation and processing for metabolomics and bioinformatics data analysis and Tracy Bellande for expert technical assistance. Finally, we thank the patients and caregivers for their participation and contribution to this study.

References

1011 1. Michel PP, Hirsch EC, Hunot S. Understanding Dopaminergic Cell Death Pathways in Parkinson
1012 Disease. Neuron. 2016; 90(4):675–691.
1013 2. Brundin P, Melki R, Kopito R. Prion-like transmission of protein aggregates in neurodegenerative
1014 diseases. Nat Rev Mol Cell Biol. 2010; 11(4):301-7.
1015 3. Dehay B, Bourdenx M, Gorry P, Przedborski S, Vila M, Hunot S, et al., Targeting α-synuclein for
1016 treatment of Parkinson's disease: Mechanistic and therapeutic considerations. Lancet Neurol.
1017 2015; 14(8):855–866.
1018 4. Hirsch EC, Hunot S. Neuroinflammation in Parkinson's disease: A target for neuroprotection?
1019 Lancet Neurol. 2009; 8(4):382–397.
1020 5. Heneka M T, Carson MJ, Khoury JE, Landreth GE, Brosseron F, Feinstein DL, et al.,
1021 Neuroinflammation in Alzheimer's disease. Lancet Neurol. 2015; 14(4):388–405.
1022 6. Lim S, Chun Y, Lee JS, Lee S-J. Neuroinflammation in Synucleinopathies. Brain Pathol. 2016;
1023 26(3):404–409.
1024 7. Panicker N, Sarkar S, Harischandra DS, Neal M, Kam T-I, Jin H, et al., Fyn kinase regulates misfolded
1025 α-synuclein uptake and NLRP3 inflammasome activation in microglia. J Exp Med. 2019;
1026 216(6):1411–1430.
1027 8. Scheiblich H, Bousset L, Schwartz S, Griep A, Latz E, Melki R, et al., Microglial NLRP3
1028 Inflammasome Activation upon TLR2 and TLR5 Ligation by Distinct α-Synuclein Assemblies. J
1029 Immunol. 2021; 207(8):2143–2154.
1030 9. Scheiblich H, Dansokho C, Mercan D, Schmidt SV, Bousset L, Wischhof L, et al., Microglia jointly
1031 degrade fibrillar alpha-synuclein cargo by distribution through tunneling nanotubes. Cell. 2021;
1032 184(20):5089-5106.
1033 10. Bousset L, Pieri L, Ruiz-Arlandis G, Gath J, Jensen PH, Habenstein, et al., Structural and functional
1034 characterization of two alpha-synuclein strains. Nat Commun. 2013; 4(1):2575.
1035 11. Gribaudo S, Tixador P, Bousset L, Fenyi A, Lino P, Melki R, et al., Propagation of α-Synuclein strains
1036 within human reconstructed neuronal network. Stem Cell Rep. 2019; 12(2):230-244.
1037 12. Shrivastava AN, Bousset L, Renner M, Redeker V, Savistchenko J, Triller A, et al., Differential
1038 membrane binding and seeding of distinct α-Synuclein fibrillar polymorphs. Biophys J. 2020;
1039 118(6):1301-1320.
1040 13. Peelaerts W, Bousset L, Van der Perren A, Moskalyuk A, Pulizzi R, Giugliano M, et al., α-Synuclein
1041 strains cause distinct synucleinopathies after local and systemic administration. Nature. 2015;
1042 522(7556):340–344.
1043 14. Rey NL, Bousset L, George S, Madaj Z, Meyerdirk L, Schulz E, et al., α-Synuclein conformational
1044 strains spread, seed and target neuronal cells differentially after injection into the olfactory bulb.
1045 Acta Neuropathol Commun. 2019; 7(1):221.
1046 15. Van der Perren A, Gelders G, Fenyi A, Bousset L, Brito F, Peelaerts W, et al., The structural
1047 differences between patient-derived α-synuclein strains dictate characteristics of Parkinson's
1048 disease, multiple system atrophy and dementia with Lewy bodies. Acta Neuropathol. 2020;
1049 139(6):977–1000.
1050 16. Landureau M, Redeker V, Bellande T, Eyquem S, Melki R. The differential solvent exposure of N-
1051 terminal residues provides "fingerprints" of alpha-synuclein fibrillar polymorphs. J Biol Chem.
1052 2021; 296:100737.
1053 17. Song S-Y, Kim I-S, Koppula S, Park J-Y, Kim B-W, Yoon S-H, et al., 2-Hydroxy-4-Methylbenzoic
1054 Anhydride Inhibits Neuroinflammation in Cellular and Experimental Animal Models of Parkinson's
1055 Disease. Int J Mol Sci. 2020; 21(21):8195.

1056 18. Tu D, Gao Y, Yang R, Guan T, Hong J-S, Gao H-M. The pentose phosphate pathway regulates chronic
1057 neuroinflammation and dopaminergic neurodegeneration. J Neuroinflammation. 2019; 16(1):1–
1058 17.
1059 19. Perry VH, Nicoll JAR, Holmes C. Microglia in neurodegenerative disease. Nat Rev Neurol. 2010;
1060 6(4):193–201.
1061 20. Chiu IM, Morimoto ETA, Goodarzi H, Liao JT, O'Keeffe S, Phatnani HP, et al., A Neurodegeneration-
1062 Specific Gene-Expression Signature of Acutely Isolated Microglia from an Amyotrophic Lateral
1063 Sclerosis Mouse Model. Cell Rep. 2013; 4(2):385–401.
1064 21. Xue J, Schmidt SV, Sander J, Draffehn A, Krebs W, Quester I, et al., Transcriptome-Based Network
1065 Analysis Reveals a Spectrum Model of Human Macrophage Activation. Immunity. 2014; 40(2):274–
1066 288.
1067 22. Ciofani M, Madar A, Galan C, Sellars M, Mace K, Pauli F, et al., A Validated Regulatory Network for
1068 Th17 Cell Specification. Cell. 2012; 151(2):289–303.
1069 23. Marino MW, Dunn A, Grail D, Inglese M, Noguchi Y, Richards E, et al., Characterization of tumor
1070 necrosis factor-deficient mice. Proc Natl Acad Sci USA. 1997; 94(15):8093–8098.
1071 24. Popov A, Abdullah Z, Wickenhauser C, Saric T, Driesen J, Hanisch F-G, et al., Indoleamine 2,3-
1072 dioxygenase–expressing dendritic cells form suppurative granulomas following Listeria
1073 monocytogenes infection. J Clin Invest. 2006; 116(12):3160–3170.
1074 25. Reiling N, Hölscher C, Fehrenbach A, Kröger S, Kirschning CJ, Goyert S, et al., Cutting Edge: Toll-Like
1075 Receptor (TLR)2- and TLR4-Mediated Pathogen Recognition in Resistance to Airborne Infection
1076 with *Mycobacterium tuberculosis*. J Immunol. 2002; 169(7):3480–3484.
1077 26. Shay JES, Celeste Simon M. Hypoxia-inducible factors: Crosstalk between inflammation and
1078 metabolism. Sem Cell Dev Biol. 2012; 23(4):389–394.
1079 27. Doorn KJ, Moors T, Drukarch B, van de Berg WD, Lucassen PJ, van Dam, A-M. Microglial
1080 phenotypes and toll-like receptor 2 in the substantia nigra and hippocampus of incidental Lewy
1081 body disease cases and Parkinson's disease patients. Acta Neuropathol Commun. 2014; 2(1):90.
1082 28. Hunot S, Boissière F, Faucheux B, Brugg B, Mouatt-Prigent A, Agid Y et al., Nitric oxide synthase
1083 and neuronal vulnerability in parkinson's disease. Neuroscience. 1996; 72(2):355–363.
1084 29. Wu Y-R, Feng I-H, Lyu R-K, Chang K-H, Lin Y-Y, Chan H et al., Tumor necrosis factor-α promoter
1085 polymorphism is associated with the risk of Parkinson's disease. Am J Med Genet. 2007;
1086 144B(3):300–304.
1087 30. Sepulveda-Diaz JE, Ouidja MO, Socias SB, Hamadat S, Guerreiro S, Raisman-Vozari R, et al., A
1088 simplified approach for efficient isolation of functional microglial cells: Application for modeling
1089 neuroinflammatory responses *in vitro*: Simplified Approach for Microglia Isolation. Glia. 2016;
1090 64(11):1912–1924.
1091 31. Tourville A, Akbar D, Corti O, Prehn JHM, Melki R, Hunot S, et al., Modelling α-Synuclein
1092 Aggregation and Neurodegeneration with Fibril Seeds in Primary Cultures of Mouse Dopaminergic
1093 Neurons. Cells. 2022; 11(10):1640.
1094 32. Pozzi D, Ban J, Iseppon F, Torre V. An improved method for growing neurons: Comparison with
1095 standard protocols. J Neurosci Methods. 2017; 15:280:1-10.
1096 33. Rook GAW, Steele J, Umar S, Dockrell HM. A simple method for the solubilisation of reduced NBT,
1097 and its use as a colorimetric assay for activation of human macrophages by γ-interferon. J
1098 Immunol Methods. 1985; 82(1):161–167.
1099 34. Love MI, Huber W, Anders S. Moderated estimation of fold change and dispersion for RNA-seq
1100 data with DESeq2. Genome Biol. 2014; 15(12):550.

1101 35. Chen EY, Tan CM, Kou Y, Duan Q, Wang Z, Meirelles GV, et al., Enrichr: Interactive and collaborative
1102 HTML5 gene list enrichment analysis tool. BMC Bioinform. 2013; 14(1):128.
1103 36. Kuleshov MV, Jones MR, Rouillard AD, Fernandez NF, Duan Q, Wang Z, et al., Enrichr: A
1104 comprehensive gene set enrichment analysis web server 2016 update. Nucleic Acids Res. 2016;
1105 44(W1):W90–W97.
1106 37. Xie Z, Bailey A, Kuleshov MV, Clarke DJB., Evangelista JE, Jenkins SL, et al., Gene Set Knowledge
1107 Discovery with Enrichr. Curr Protoc. 2021; 1(3).
1108 38. Garali I, Adanyeguh IM, Ichou F, Perlbarg V, Seyer A, Colsch B, et al., A strategy for multimodal data
1109 integration: Application to biomarkers identification in spinocerebellar ataxia. Brief Bioinform.
1110 2018; 19(6):1356–1369.
1111 39. Giacomoni F, Le Corguille G, Monsoor M, Landi M, Pericard P, Petera M, et al.,
1112 Workflow4Metabolomics: A collaborative research infrastructure for computational
1113 metabolomics. Bioinformatics. 2015; 31(9):1493–1495.
1114 40. Smith CA, Want EJ, O'Maille G, Abagyan R, Siuzdak G. XCMS: Processing Mass Spectrometry Data
1115 for Metabolite Profiling Using Nonlinear Peak Alignment, Matching, and Identification. Anal Chem.
1116 2006; 78(3):779–787.
1117 41. Tautenhahn R, Patti GJ, Rinehart D, Siuzdak G. XCMS Online: A Web-Based Platform to Process
1118 Untargeted Metabolomic Data. Anal Chem. 2012; 84(11):5035–5039.
1119 42. Dunn WB, Broadhurst D, Begley P, Zelena E, Francis-McIntyre S, Anderson N, et al., Procedures for
1120 large-scale metabolic profiling of serum and plasma using gas chromatography and liquid
1121 chromatography coupled to mass spectrometry. Nat Protoc. 2011; 6(7):1060–1083.
1122 43. Want EJ, Wilson ID, Gika H, Theodoridis G, Plumb RS, Shockcor J, et al., Global metabolic profiling
1123 procedures for urine using UPLC–MS. Nat Protoc. 2010; 5(6):1005–1018.
1124 44. Dunn WB, Wilson ID, Nicholls AW, Broadhurst D. The importance of experimental design and QC
1125 samples in large-scale and MS-driven untargeted metabolomic studies of humans. Bioanalysis.
1126 2012; 4(18): 2249–2264.
1127 45. Veselkov KA, Vingara LK, Masson P, Robinette SL, Want E, Li JV, et al., Optimized Preprocessing of
1128 Ultra-Performance Liquid Chromatography/Mass Spectrometry Urinary Metabolic Profiles for
1129 Improved Information Recovery. Anal Chem. 2011; 83(15):5864–5872.
1130 46. Saeed AI, Sharov V, White J, Li J, Liang W, Bhagabati N, et al., TM4: A Free, Open-Source System for
1131 Microarray Data Management and Analysis. BioTechniques. 2003; 34(2):374–378.
1132 47. Benjamini Y, Hochberg Y. Controlling the False Discovery Rate: A Practical and Powerful Approach
1133 to Multiple Testing. J. R. Stat. Soc. 1995; 57(1):289–300.
1134 48. Ohgidani M, Kato TA, Setoyama D, Sagata N, Hashimoto R, Shigenobu K, et al., Direct induction of
1135 ramified microglia-like cells from human monocytes: Dynamic microglial dysfunction in Nasu-
1136 Hakola disease. Sci Rep. 2015; 4(1):4957.
1137 49. Döring C, Regen T, Gertig U, van Rossum D, Winkler A, Saiepour N, et al., A presumed antagonistic
1138 LPS identifies distinct functional organization of TLR4 in mouse microglia. Glia. 2017; 65(7):1176–
1139 1185.
1140 50. dos-Santos-Pereira M, Acuña L, Hamadat S, Rocca J, González-Lizárraga F, Chehín R, et al.,
1141 Microglial glutamate release evoked by α-synuclein aggregates is prevented by dopamine. Glia.
1142 2018; 66(11):2353–2365.
1143 51. Ginhoux F, Greter M, Leboeuf M, Nandi S, See P, Gokhan S, et al., Fate Mapping Analysis Reveals
1144 That Adult Microglia Derive from Primitive Macrophages. Science. 2010; 330(6005):841–845.

1145 52. Choi I, Zhang Y, Seegobin S P, Pruvost M, Wang Q, Purtell K, et al., Microglia clear neuron-released
1146 α-synuclein via selective autophagy and prevent neurodegeneration. Nat Commun. 2020;
1147 11(1):1386.
1148 53. Fellner L, Irschick R, Schanda K, Reindl M, Klimaschewski L, Poewe W, et al., Toll-like receptor 4 is
1149 required for α-synuclein dependent activation of microglia and astroglia. Glia. 2013; 61(3):349–
1150 360.
1151 54. Gustot A, Gallea JI, Sarroukh R, Celej MS, Ruysschaert J-M, Raussens V. Amyloid fibrils are the
1152 molecular trigger of inflammation in Parkinson's disease. Biochem J. 2015; 471(3):323–333.
1153 55. Lim S, Chun Y, Lee JS, Lee SJ. Neuroinflammation in Synucleinopathies. Brain Pathol. 2016;
1154 26(3):404-9.
1155 56. Drier Y, Sheffer M, Domany E. Pathway-based personalized analysis of cancer. Proc Natl Acad Sci.
1156 USA. 2013; 110(16):6388–6393.
1157 57. Lewerenz J, Hewett SJ, Huang Y, Lambros M, Gout PW, Kalivas PW, et al., The Cystine/Glutamate
1158 Antiporter System xc-in Health and Disease: From Molecular Mechanisms to Novel Therapeutic
1159 Opportunities. Antioxid Redox Signal. 2013; 18(5):522–555.
1160 58. Rodríguez-Prados JC, Través PG, Cuenca J, Rico D, Aragonés J, Martín-Sanz P, et al., Substrate Fate
1161 in Activated Macrophages: A Comparison between Innate, Classic, and Alternative Activation. J
1162 Immunol. 2010; 185(1):605–614.
1163 59. Orihuela R, McPherson CA, Harry GJ. Microglial M1/M2 polarization and metabolic states:
1164 Microglia bioenergetics with acute polarization. Br J Pharmacol. 2016; 173(4):649–665.
1165 60. Angajala A, Lim S, Phillips JB, Kim J-H, Yates C, You Z, et al., Diverse roles of mitochondria in
1166 immune responses: novel insights into immuno-metabolism. Front Immunol. 2018; 9:1605.
1167 61. Galatro TF, Holtman IR, Lerario AM, Vainchtein ID, Brouwer N, Sola PR, et al., Transcriptomic
1168 analysis of purified human cortical microglia reveals age-associated changes. Nat Neurosci. 2017;
1169 20(8):1162–1171.
1170 62. Mizutani M, Pino PA, Saederup N, Charo IF, Ransohoff RM, Cardona AE. The Fractalkine Receptor
1171 but Not CCR2 Is Present on Microglia from Embryonic Development throughout Adulthood. J
1172 Immunol. 2012; 188(1):29–36.
1173 63. Wang J, Wang F, Mai D, Qu, S. Molecular Mechanisms of Glutamate Toxicity in Parkinson's Disease.
1174 Front Neurosci. 2020; 14:585584.
1175 64. Colonna M, Butovsky O. Microglia Function in the Central Nervous System During Health and
1176 Neurodegeneration. Annu Rev Immunol. 2017; 35(1):441–468.
1177 65. Prinz M, Jung S, Priller J. Microglia Biology: One Century of Evolving Concepts. Cell. 2019; 179(2):
1178 292–311.
1179 66. Ransohoff RM, Perry VH. Microglial Physiology: Unique Stimuli, Specialized Responses. Ann Rev
1180 Immunol. 2009; 27(1):119–145.
1181 67. Bodea L-G, Wang Y, Linnartz-Gerlach B, Kopatz J, Sinkkonen L, Musgrove R, et al.,
1182 Neurodegeneration by Activation of the Microglial Complement-Phagosome Pathway. J Neurosci.
1183 2014; 34(25):8546–8556.
1184 68. Donat CK, Scott G, Gentleman SM, Sastre M. Microglial Activation in Traumatic Brain Injury.
1185 Frontiers in Aging Neurosci. 2017; 9:208.
1186 69. Lull ME, Block ML. Microglial activation and chronic neurodegeneration. Neurotherapeutics. 2010;
1187 7(4):354–365.
1188 70. Ouchi Y, Yagi S, Yokokura M, Sakamoto M. Neuroinflammation in the living brain of Parkinson's
1189 disease. Parkinsonism Relat Disord. 2009; 15:S200–S204.

1190 71. Daniele SG, Béraud D, Davenport C, Cheng K, Yin H, Maguire-Zeiss KA. Activation of MyD88-
1191 dependent TLR1/2 signaling by misfolded α-synuclein, a protein linked to neurodegenerative
1192 disorders. Sci Signal. 2015; 8(376).
1193 72. Codolo G, Plotegher N, Pozzobon T, Brucale M, Tessari I, Bubacco L, et al., Triggering of
1194 Inflammasome by Aggregated α–Synuclein, an Inflammatory Response in Synucleinopathies. PLoS
1195 ONE. 2013; 8(1):e55375.
1196 73. Feng Y, Zheng C, Zhang Y, Xing C, Cai W, Li R et al., Triptolide Inhibits Preformed Fibril-Induced
1197 Microglial Activation by Targeting the MicroRNA155-5p/SHIP1 Pathway. Oxid Med Cell Longev.
1198 2019; 1–13.
1199 74. Kim C, Ho D-H, Suk J-E, You S, Michael S, Kang J, et al., Neuron-released oligomeric α-synuclein is
1200 an endogenous agonist of TLR2 for paracrine activation of microglia. Nat Commun. 2013;
1201 4(1):1562.
1202 75. Guerrero-Ferreira R, Taylor NM, Arteni AA, Kumari P, Mona D, Ringler P, et al., Two new
1203 polymorphic structures of human full-length alpha-synuclein fibrils solved by cryo-electron
1204 microscopy. Elife. 2019; 8:e48907.
1205 76. Burger D, Fenyi A, Bousset L, Stahlberg H, Melki R. Cryo-EM structure of alpha-synuclein fibrils
1206 amplified by PMCA from PD and MSA patient brains. bioRxiv.
1207 2021; 451588; doi: https://doi.org/10.1101/2021.07.08.451588.
1208 77. Shahnawaz M, Mukherjee A, Pritzkow S, Mendez N, Rabadia P, Liu X, et al., Discriminating α-
1209 synuclein strains in Parkinson's disease and multiple system atrophy. Nature. 2020;
1210 578(7794):273–277.
1211 78. Aoki T, Narumiya S. Prostaglandins and chronic inflammation. Trends Pharmacol Sci. 2012;
1212 33(6):304–311.
1213 79. Balkwill F. Tumor necrosis factor and cancer. Nat. Rev Cancer. 2009; 9(5):361–371.
1214 80. Mattammal MB, Strong R, Lakshmi VM, Chung HD, Stephenson AH. Prostaglandin H Synthetase-
1215 Mediated Metabolism of Dopamine: Implication for Parkinson's Disease. J Neurochem. 2002;
1216 64(4):1645–1654.
1217 81. Mogi M, Harada M, Riederer P, Narabayashi H, Fujita K, Nagatsu T. Tumor necrosis factor-α (TNF-α)
1218 increases both in the brain and in the cerebrospinal fluid from parkinsonian patients. Neurosci
1219 Lett. 1994; 165(1–2):208–210.
1220 82. Teismann P, Tieu K, Choi D-K, Wu D-C, Naini A, Hunot S, et al., Cyclooxygenase-2 is instrumental in
1221 Parkinson's disease neurodegeneration. Proc Natl Acad Sci USA. 2003; 100(9):5473–5478.
1222 83. Tansey MG, Goldberg MS. Neuroinflammation in Parkinson's disease: Its role in neuronal death
1223 and implications for therapeutic intervention. Neurobiol Dis. 2010; 37(3):510–518.
1224 84. Teismann P, Tieu K, Cohen O, Choi D-K, Wu DC, Marks D, et al., Pathogenic role of glial cells in
1225 Parkinson's disease. Mov Disord. 2003; 18(2):121–129.
1226 85. Locati M, Curtale G, Mantovani A. Diversity, Mechanisms, and Significance of Macrophage
1227 Plasticity. Ann Rev Pathol. 2020; 15(1):123–147.
1228 86. Mesci P, Zaïdi S, Lobsiger CS, Millecamps S, Escartin C, Seilhean D, et al., System xC− is a mediator
1229 of microglial function and its deletion slows symptoms in amyotrophic lateral sclerosis mice. Brain.
1230 2015; 138(1):53–68.
1231 87. Qin S, Colin C, Hinners I, Gervais A, Cheret C, Mallat M. System Xc- and Apolipoprotein E Expressed
1232 by Microglia Have Opposite Effects on the Neurotoxicity of Amyloid-beta Peptide 1-40. J Neurosci.
1233 2006; 26(12):3345–3356.

1234 88. Lavaur J, Le Nogue D, Lemaire M, Pype J, Farjot G, Hirsch EC, et al., The noble gas xenon provides
1235 protection and trophic stimulation to midbrain dopamine neurons. J Neurochem. 2017;
1236 142(1):14–28.
1237 89. Ambrosi G, Cerri S, Blandini F. A further update on the role of excitotoxicity in the pathogenesis of
1238 Parkinson's disease. J Neural Transm. 2014; 121(8):849–859.
1239 90. Massie A, Schallier A, Mertens B, Vermoesen K, Bannai S, Sato H, et al., Time-dependent changes
1240 in striatal xCT protein expression in hemi-Parkinson rats. NeuroReport. 2008; 19(16):1589–1592.
1241 91. Massie A, Schallier A, Kim SW, Fernando R, Kobayashi S, Beck H, et al., Dopaminergic neurons of
1242 system x(c)$^{-}$-deficient mice are highly protected against 6-hydroxydopamine-induced toxicity.
1243 FASEB J. 2011; 25(4):1359–1369.
1244 92. Bentea E, Sconce MD, Churchill MJ, Van Liefferinge J, Sato H, Meshul CK, et al., MPTP-induced
1245 parkinsonism in mice alters striatal and nigral xCT expression but is unaffected by the genetic loss
1246 of xCT. Neurosci Lett. 2015; 593:1–6.
1247 93. Kapralov AA, Yang Q, Dar HH, Tyurina YY, Anthonymuthu TS, Kim R, et al., Redox lipid
1248 reprogramming commands susceptibility of macrophages and microglia to ferroptotic death. Nat
1249 Chem Biol. 2020; 16(3):278–290.
1250 94. Pereira M, Chen T-D, Buang N, Olona A, Ko J-H, Prendecki M, et al., Acute Iron Deprivation
1251 Reprograms Human Macrophage Metabolism and Reduces Inflammation In Vivo. Cell Rep. 2019;
1252 28(2):498-511.e5.
1253 95. McCarthy RC, Sosa JC, Gardeck AM, Baez AS, Lee C-H, Wessling-Resnick M. Inflammation-induced
1254 iron transport and metabolism by brain microglia. J Biol Chem. 2018; 293(20):7853–7863.
1255 96. Guo J-J, Yue F, Song D-Y, Bousset L, Liang X, Tang J, et al., Intranasal administration of α-synuclein
1256 preformed fibrils triggers microglial iron deposition in the substantia nigra of Macaca fascicularis.
1257 Cell Death Dis. 2021; 12(1):81.
1258 97. Ryan SK, Zelic M, Han Y, Teeple E, Chen L, Sadeghi M, et al., Microglia ferroptosis is regulated by
1259 SEC24B and contributes to neurodegeneration. Nat Neurosci. 2023; 26:12-26.
1260 98. Kenkhuis B, van Eekeren M, Parfitt DA, Ariyurek Y, Banerjee P, Priller J, et al., Iron accumulation
1261 induces oxidative stress, while depressing inflammatory polarization in human iPSC-derived
1262 microglia. Stem Cell Rep. 2022; 17:1351–1365.
1263 99. Warburg O. On respiratory impairment in cancer cells. Science. 1956; 124:269–70.
1264 100. Kim CC, Nakamura MC, Hsieh CL. Brain trauma elicits non-canonical macrophage activation states.
1265 J Neuroinflammation. 2016; 13(1):117.
1266 101. Morganti JM, Riparip L-K, Rosi S. Call Off the Dog(ma): M1/M2 polarization Is concurrent following
1267 traumatic brain injury. PLoS ONE. 2016; 11(1):e0148001.
1268 102. Szulzewsky F, Pelz A, Feng X, Synowitz M, Markovic D, Langmann T, et al., Glioma-Associated
1269 Microglia/Macrophages Display an Expression Profile Different from M1 and M2 Polarization and
1270 Highly Express Gpnmb and Spp1. PLoS ONE. 2015; 10(2):e0116644.
1271 103. Keren-Shaul H, Spinrad A, Weiner A, Matcovitch-Natan O, Dvir-Szternfeld R, Ulland TK, et al., A
1272 Unique Microglia Type Associated with Restricting Development of Alzheimer's Disease. Cell.
1273 2017; 169(7):1276-1290.
1274 104. McFarland KN, Ceballos C, Rosario A, Ladd T, Moore B, Golde G, et al., Microglia show differential
1275 transcriptomic response to Aβ peptide aggregates ex vivo and in vivo. Life Sci Alliance. 2021;
1276 4(7):e202101108.